HHS Public Access

Author manuscript

Toxicol Appl Pharmacol. Author manuscript; available in PMC 2016 April 01.

Published in final edited form as:

Toxicol Appl Pharmacol. 2015 April 1; 284(1): 65–78. doi:10.1016/j.taap.2015.01.022.

Motoneuron axon pathfinding errors in zebrafish: Differential effects related to concentration and timing of nicotine exposure

Evdokia Menelaou[1,*], **Latoya T. Paul**[1], **Surangi N. Perera**[2], and **Kurt R. Svoboda**[1,2]

[1]Department of Biological Sciences, Louisiana State University, Baton Rouge, LA 70803

[2]Joseph J. Zilber School of Public Health, University of Wisconsin-Milwaukee, Milwaukee 53205

Abstract

Nicotine exposure during embryonic stages of development can affect many neurodevelopmental processes. In the developing zebrafish, exposure to nicotine was reported to cause axonal pathfinding errors in the later born secondary motoneurons (SMN). These alterations in SMN axon morphology coincided with muscle degeneration at high nicotine concentrations (15–30μM). Previous work showed that the paralytic mutant zebrafish known as *sofa potato*, exhibited nicotine-induced effects onto SMN axons at these high concentrations but in the absence of any muscle deficits, indicating that pathfinding errors could occur independent of muscle effects.

In this study, we used varying concentrations of nicotine at different developmental windows of exposure to specifically isolate its effects onto subpopulations of motoneuron axons. We found that nicotine exposure can affect SMN axon morphology in a dose-dependent manner. At low concentrations of nicotine, SMN axons exhibited pathfinding errors, in the absence of any nicotine-induced muscle abnormalities. Moreover, the nicotine exposure paradigms used affected the 3 subpopulations of SMN axons differently, but the dorsal projecting SMN axons were primarily affected. We then identified morphologically distinct pathfinding errors that best described the nicotine-induced effects on dorsal projecting SMN axons. To test whether SMN pathfinding was potentially influenced by alterations in the early born primary motoneuron (PMN), we performed dual labeling studies, where both PMN and SMN axons were simultaneously labeled with antibodies. We show that only a subset of the SMN axon pathfinding errors coincided with abnormal PMN axonal targeting in nicotine-exposed zebrafish. We conclude that nicotine exposure can exert differential effects depending on the levels of nicotine and developmental exposure window.

Keywords

axonal pathfinding; muscle degeneration; embryonic spinal cord; dual labeling

Correspondence: Kurt R. Svoboda, svobodak@uwm.edu, Phone: 414-382-1707, Fax: 414-382-1705.

*__Current address:__

Department of Neurobiology, Northwestern University, Evanston, IL 60208

Introduction

Exposure to nicotine, a potent cholinergic agonist, during embryogenesis causes paralysis in zebrafish embryos and larvae. The nicotine-induced paralysis coincides with pronounced alterations in motoneuron (Svoboda et al., 2002; Menelaou and Svoboda, 2009) and muscle development (Welsh et al., 2009). In developing chick and zebrafish, motoneuron axon growth and muscle development occur simultaneously and involve activity-dependent mechanisms (Hanson and Landmesser, 2004; Plazas et al., 2013), calcium signaling (Brennan et al., 2005), and multiple myotome-derived cues (Zeller et al., 2002; Schweitzer et al. 2005; Schneider and Granato, 2006; Palaisa and Granato, 2007).

In the presence of nicotine, both neuronal and muscle tissues can be severely affected by activation of nicotinic acetylcholine receptors (nAChRs) (Welsh et al., 2009). In zebrafish embryos, acetylcholine-generated calcium transients regulate muscle fiber development (Brennan et al., 2005). Following prolonged activation of skeletal muscle via over-activation of nAChRs present on muscle, motor axon defects and muscle degeneration occur (Lefebvre et al., 2004, Behra et al., 2002), possibly via excitotoxic mechanisms due to increased calcium levels in the muscle (Engel et al., 1982; Gomez et al., 2002). This evidence supports a direct action of nicotine on muscle fiber development via the activation of muscle-specific AChRs.

Sofa potato zebrafish mutants that lack functional skeletal muscle nAChRs (Ono et al., 2001) exhibited secondary motoneuron (SMN) pathfinding errors without any effects on muscle development following embryonic nicotine exposure (15 and 30μM, Welsh et al., 2009). This suggested that nicotine-induced neuronal and muscle effects can occur independently from each other and that muscle fibers are not the sole substrate that nicotine acts upon to alter SMN anatomy. These results also indicate that nicotine can directly affect cells within the nervous system.

In the following experiments, zebrafish embryos were exposed to different concentrations of nicotine at different developmental time windows to determine if nicotine could directly alter motoneuron axon morphology, bypassing any muscle defects. The results show that the motoneuron and muscle effects uncouple in a dose-dependent manner as a result of either short or long duration nicotine exposure window. We then identified four distinct, motoneuron axon pathfinding errors that were caused by nicotine exposure, specifically affecting dorsal projecting SMN axons. Next, to demonstrate whether these nicotine-induced effects were specific to dorsal projecting SMNs, we also examined primary motoneuron (PMN) axons which develop first and extend their axons in the muscle prior to SMNs (Myers et al., 1986). This became possible following the characterization of a previously described antibody developed against the zebrafish β_2 nAChR subunit (Welsh et al., 2009). We found that this antibody specifically recognizes PMN axons that project ventrally (Caudal Primary, CaP) and dorsally (Middle Primary, MiP) into the muscle. With this antibody in our toolbox, we were able to simultaneously assess the pathfinding of both PMN and SMN axons in the same nicotine-exposed zebrafish. We demonstrate that nicotine exposure can affect PMN axon pathfinding which can potentially influence the later born

SMN axon morphologies. In addition, a subset of the distinct nicotine-induced SMN phenotypes occurred independent of any PMN axon defects suggesting that nicotine exposure can specifically affect SMN axon pathfinding.

Materials and Methods

Zebrafish Maintenance

Animal protocols were approved by the Institutional Animal Care and Use Committees at Louisiana State University and the University of Wisconsin-Milwaukee. Adult wild-type and transgenic (Tg(*isl1*:GFP), *parg*^{mn2Et} and Tg(*gata2*:GFP) fish were maintained at ~28°C with a lighting schedule of 14 h light and 10 h dark. Fertilized eggs were obtained from natural spawnings of adult zebrafish according to the *Zebrafish Book* (Westerfield, 1995). Embryos were collected within 3 hours of spawning, rinsed, and placed into 100 mm Petri dishes containing embryo medium (Westerfield, 1995).

Nicotine Exposures

(−)-Nicotine was purchased from Sigma (St. Louis, Missouri, USA, catalog # N3876-5ml) and stock solutions (31.2 mM) were made fresh daily in distilled water. The stock solution was then diluted in embryo medium (pH 7.2) to obtain the desired final concentrations. Zebrafish embryos while in their chorions were exposed to nicotine (1, 5, 15, and 30μM) from 12–30 and 22–72 hours post fertilization (hpf). For all nicotine exposures, the number of embryos exposed for each group was the same. At 48 hpf, all nicotine-exposed and stage-matched control embryos were manually dechorionated and at 72 hpf (larval stage), were anaesthetized in MS222 and fixed in 4% paraformaldehyde.

Immunohistochemistry

Whole mount immunohistochemistry was carried out in zebrafish ranging in age from 28 hpf to 72 hpf that were first fixed in 4% paraformaldehyde overnight at 2–4°C and then stored in PBST (PBS containing 0.1% Tween 20). After permeabilization (See Svoboda et al., 2001 for details), they were incubated in a primary antibody overnight at 2–4°C. The monoclonal antibodies zn5 (also known as zn8) (dilution 1:500), F59 (dilutions 1:100–1:250) and znp-1 (dilution 1:250) were obtained from the Developmental Studies Hybridoma Bank (The University of Iowa, Iowa) and were used to reveal secondary motoneuron somata and their axons (Fashena and Westerfield, 1999), slow muscle fibers (Devoto et al., 1996), and primary motoneuron axons (Zeller and Granato, 1999), respectively. Generation and characterization of the polyclonal anti-β_2 nAChR antibody has been described previously (Welsh et al., 2009) and was used at a dilution of 1:250. From here onward, it will be referred to as *anti-chrn2b*. The following day, the embryos/larvae were washed in PBST for 90 minutes and then incubated for another 90 minutes in an anti-mouse or anti-rabbit fluorescent secondary antibody conjugated to Alexa 546 or Alexa 488 (1:1000 dilution in PBST; Molecular Probes, Eugene, OR). The samples were then rinsed in PBST for another 60 minutes and prepared for image analysis.

For dual labeling experiments, fish were first incubated with the primary antibody, znp-1 or zn5, and then followed by their corresponding anti-mouse fluorescent secondary antibody.

Next, fish were washed for 90 minutes in PBST and then incubated with the *anti-chrn2b* antibody overnight at 2–4°C. The next day, following another 90-minute wash in PBST, the anti-rabbit fluorescent secondary antibody was added. Lastly, the fish were rinsed in PBST for at least 60 minutes prior to imaging.

Image Acquisition and Analysis of Morphological Data

Zebrafish processed via immunohistochemistry were laterally mounted on a slide in PBST, lightly cover slipped, and sealed. Single focal plane images (zn5 labeled fish) and image stacks (zn5, znp-1, *anti-chrn2b* and F59 labeled fish) were obtained with an Orca ER CCD camera mounted to a Zeiss inverted microscope (Axiovert 200M or Axio Observer) equipped with epifluorescence and a Zeiss ApoTome (Carl Zeiss). Images were acquired with a 20× dry (0.6 N.A, 0.8 N.A), a 25× water (0.8 N.A.), or a 40× oil (1.3 N.A.) objective. Multiple single focal plane images were acquired for each fish capturing motoneuron axon morphologies from both sides within each body segment. Image stacks were acquired to reveal high-resolution motoneuron axon morphology using volume-rendering software (Imaris 5.7.2, Bitplane Inc., Saint Paul, MN).

Evaluation of motoneuron axon morphology following different nicotine exposure paradigms was performed on single focal plane images taken from multiple hemisegments for control and nicotine-exposed fish. For every fish, we focused our analysis between the 6^{th} and 20^{th} body segment. Each body segment consists of two hemisegments, one on each side of the body. The number of hemisegments imaged and analyzed per fish varied depending on the quality of the fish's lateral mount on the slide.

Each hemisegment typically has one motoneuron nerve bundle that exits spinal cord and its axons take three distinct trajectories to the periphery; dorsal, ventral and mediolateral (see Fig. 1C). zn5 labeling was used to label SMN axons and if a hemisegment possessed SMN axon errors in any of the three axonal trajectories, that hemisegment was then considered abnormal. The number of normal hemisegments over the total number of hemisegments analyzed per fish was then expressed as a percentage. Each nicotine exposure paradigm was replicated multiple times (5 experiments for 22–72 hpf, Supplemental Fig. 1A; 3 experiments for 12–30 hpf; Supplemental Fig. 1B).

To quantify the effects of nicotine exposure on individual axonal trajectories (dorsal, ventral and mediolateral), a subset of the fish analyzed for Figure 2Fi (22–72 hpf exposure window) and the fish analyzed for Figure 2Fii (12–30 hpf exposure window) were used. Hence, the quantification shown in Table 1 and the subsequent motoneuron phenotyping of the dorsal projecting SMN axons was performed from the same experimental dataset for each nicotine exposure paradigm. For Table 1, each hemisegment was evaluated for errors in any of the three main trajectories (dorsal, ventral and mediolateral). For example, the number of hemisegments that possessed abnormal dorsal projecting axons was divided by the total number of hemisegments analyzed and was then expressed as a percentage. This quantification revealed the relative effects of nicotine on different axonal projections.

Evaluation of muscle fiber morphology was performed using high-resolution image stacks following F59 labeling (Welsh et al., 2009). Slow muscle measurements (fiber widths) were

acquired using Axiovision 4.7/4.8 (Carl Zeiss) software. For each fish, multiple slow muscle fibers were measured but only a single measurement was taken for a given fiber (29.7 ± 5.8 fibers/fish; mean ± standard deviation). All of the measurements were taken from 2–3 consecutive hemisegments in the mid body over the yolk sac extension, corresponding to body segments 10–15. Each measurement was arbitrarily taken from the fiber and we avoided taking measurements from fibers close to the segmental boundary or from muscle fibers adjacent to the horizontal myoseptum.

For the characterization of the *anti-chrn2b* antibody, image stacks were acquired to reveal the *anti-chrn2b* labeling in different transgenic lines or following dual labeling with either zn5 or znp-1 antibodies (Supplemental Table 1). Multiple segments from several fish were imaged to capture motoneuron morphologies at different developmental stages.

Representative high-resolution photomicrographs shown in the figures were acquired using volume-rendering software (Imaris 5.7.2, Bitplane Inc., Saint Paul, MN). Images were cropped using Photoshop 7.0 (Adobe, San Jose, CA) and CorelDraw Graphics Suite 12 (Ottawa, Ontario, CA) was used to organize the figures. All of the images are presented with rostral to the left and dorsal to the top. Cartoons were created using CorelDraw by tracing axonal trajectories from the photomicrographs.

Statistics

All data were tested for normality prior to statistical analysis. For normally distributed data, comparison of the means was performed using one-way analysis of variance (ANOVA), followed by a Holm-Sidak *post hoc* test. For data that failed the normality test, we performed a Kruskal-Wallis analysis of variance on ranks, followed by Dunn's *post hoc* test. All multiple comparisons using *post hoc* tests were performed for each nicotine group against the control. All statistical analysis was performed using SigmaPlot 11 (Systat Software Inc., San Jose, USA). For each test, we parenthetically report the degrees of freedom with its corresponding *F* or *H* values according to convention. All values are reported as means ± standard error (SE). Significance was assigned at $p < 0.05$ and is reported in the figure legends where appropriate.

Results

Previous work examining the effects of embryonic nicotine exposure on SMN axon pathfinding has utilized transgenic lines of fish (Tg(*isl1*:GFP); Tg(*gata2*:GFP)) and antibody markers (zn5) that specifically mark a large subset of secondary motoneurons and their axons (Svoboda et al., 2002, Welsh et al., 2009, Menelaou and Svoboda, 2009). These secondary motoneurons are positioned mostly in the ventral half of the spinal cord and their axons exit at mid-segmental roots where they form a fasciculated nerve fiber. This fasciculated bundle of axons then arborizes to innervate the dorsal and ventral myotomes (Myers et al., 1986; Menelaou and McLean, 2012). Specifically, the main nerve containing SMN axons can either extend dorsally (Fig. 1C, red), ventrally (Fig. 1C, blue) or mediolaterally (Fig. 1C, orange) into the myotome (axonal arborizations into the muscle are not depicted in Fig. 1C). Recently discovered, a small subset of SMNs has bifurcating axons that extend both dorsally and ventrally to arborize into the muscle (not shown on the

schematic of Fig. 1C; Menelaou and McLean, 2012). When zebrafish embryos were exposed to high concentrations of nicotine, SMN axons exhibited a variety of phenotypes which can be clearly visualized using either the Tg(*is1*:GFP) line of fish (Fig. 1B) or zn5 immunolabeling (Fig. 1A). These spatially distinct axonal trajectories were more easily visualized when the axons were labeled with zn5, which would facilitate identification of nicotine-induced alterations in either dorsal, ventral or mediolateral SMN axonal trajectories as illustrated in Figure 1D.

Embryonic nicotine exposure can specifically affect secondary motoneuron axons and bypass muscle defects

Nicotine exposure in zebrafish from 22–72 hpf has been shown to cause SMN axonal pathfinding errors and muscle degeneration at concentrations between 15 and 30μM nicotine (Svoboda et al., 2002; Welsh et al., 2009). Here, zebrafish embryos were exposed from 22–72 hpf at lower concentrations of nicotine (1 and 5μM), in addition to the previously used 15 and 30μM nicotine concentrations (Fig. 2Bi–Ei), and compared to stage-matched controls from the same cohort (Fig. 2Ai). In zebrafish embryos exposed to 1μM nicotine, the dorsal projecting SMN axons exhibited subtle misrouting effects such as incorrect navigation at the distal part of the myotome (Fig. 2Bi, filled arrow). On the other hand, zebrafish larvae exposed to 5, 15, and 30μM nicotine as embryos had SMN axons that appeared to split and project in different directions. These phenotypes were observed in the dorsal (Fig. 2Ci–Ei, filled arrows), mediolateral (Fig. 2Ci and 2Ei, arrowheads), and ventral (Fig. 2Di and 2Ei, open arrows) projecting axons.

Zebrafish myotomal segments were then examined and the abnormal SMN axon phenotypes following nicotine exposure (22–72 hpf) were quantified in individual hemisegments (Fig. 2Fi). If any one of the three main axonal trajectories (dorsal, ventral, or mediolateral projecting axons) exhibited abnormal phenotypes in axon trajectory or structure, the hemisegment was determined to have abnormal motor axon morphology. There was a reduction in the percentage of hemisegments having normal axons in nicotine-exposed fish when compared to controls (Fig. 2Fi, one-way ANOVA, $F_{(4,74)} = 76.142$, $p < 0.001$, Holm-Sidak p*ost hoc* test). This reduction in normal axons coincided with an increase in axon pathfinding errors (Fig. 2Bi–Ei) observed at all concentrations of nicotine tested.

Next, we analyzed the muscle in order to determine if the nicotine-induced effects at these different concentrations were specific to SMN axons. The morphology of slow muscle fibers was used as readout for nicotine-induced muscle defects (Welsh et al., 2009) utilizing the F59 antibody to specifically label them (Devoto et al., 1996). At high nicotine concentrations (15 and 30μM, 22–72 hpf exposure window), slow muscle morphology (Fig. 3Ci and Di) appeared abnormal which coincided with errors in SMN axonal pathfinding (Fig. 2Di–Ei, and Fi). Moreover, the overall widths of the F59-positive slow muscle fibers from nicotine-exposed (15 and 30μM) fish were thinner (Fig. 3Ci and Di) than slow muscle fibers from control fish (Fig. 3Ai and Di; Kruskal-Wallis one-way ANOVA on ranks, $H_{(4)} = 276.527$, $p < 0.001$, Dunn's p*ost hoc* test). However, at lower nicotine concentrations (1 and 5μM, Fig. 3Bi and Di), muscle morphology was normal since the slow muscle fiber widths were similar to slow muscle fiber widths of stage-matched controls (Fig. 3Di). These

findings suggest that the axonal pathfinding errors caused by 1 and 5μM nicotine concentrations could be neuronal-specific effects.

In order to determine if nicotine exposure could still exert its effects on SMN axons, even if exposed at earlier developmental stages, we performed nicotine exposures (1–30μM) from 12–30 hpf and then examined SMN axon morphology at 72 hpf. At 12 hpf, zebrafish embryos are approximately at the beginning of neurulation and well before any motoneurons extend their axons into the periphery. The nicotine exposures were terminated at 30 hpf, shortly after SMN axons begin their extension into the periphery. The embryos were then raised in fresh embryo medium to 72 hpf. In this short window of exposure, the 15 and 30μM concentrations of nicotine exposure resulted in a reduction of hemisegments with normal axons (Fig. 2Fii; one-way ANOVA, $F_{(4,25)} = 10.714$, $p < 0.001$, Holm-Sidak *post hoc* test) which coincided with an increase in axon pathfinding errors (Fig. 2Dii and 2Eii, arrows) when compared to controls. In larvae exposed to low nicotine concentrations (1 and 5μM) as embryos, SMN axons projected normally into the periphery (Fig. 2Bii and 2Cii) and were indistinguishable from their control counterparts (Fig. 2Aii). The quantification of individual experiments revealed that even the control fish appeared to possess abnormal motoneuron axon trajectories. Thus, we acknowledge that some of the nicotine-induced effects appeared subtle in nature and could be within the normal range of developmental variability. However, our experimental design accounted for such possibility by carrying out nicotine exposure experiments with fish from the same cohort. Comparisons of nicotine effects were never performed against control groups from different cohorts.

In a different set of experiments, we examined the morphology of the F59-positive, slow muscle fibers following nicotine exposure between 12–30 hpf (Fig. 3Aii–Dii). The width of slow muscle fibers from nicotine-exposed fish appeared normal with no differences in width when compared the slow muscle fibers widths from control zebrafish at all concentrations tested (Fig. 3Dii; Kruskal-Wallis one-way ANOVA on ranks ($H_{(4)} = 15.323$; p=0.004), Dunn's *post hoc* test). This suggests that SMN axon pathfinding was mostly affected only when embryos were exposed to high concentrations of nicotine between 12–30 hpf while muscle morphology still appeared normal. It further suggests that the earlier and shorter exposure window (12–30 hpf) can lead to axonal effects that are specific to motor axons and thus potentially bypass any muscle defects.

Nicotine exposure mainly affects the dorsal projecting secondary motoneuron axons

While using different nicotine exposure paradigms, it became clear that SMN axons were being affected differently. In order to investigate the differential effects of nicotine, we first focused on its effect on the different axonal trajectories (dorsal, ventral and mediolateral) but also by the nature of the pathfinding errors (Fig. 2). Based on this, we first quantified the nicotine-induced effects on SMN axons specifically for dorsal, ventral, and mediolateral projecting axons for each hemisegment. We found that among the three main motoneuron axon trajectories, nicotine exposure between 22–72 hpf primarily affected the dorsal projecting SMN axons at all nicotine concentrations (Table 1). At the higher nicotine concentrations (15 and 30μM), the ventral and mediolateral projecting axons were also significantly affected when compared to their control counterparts. Similar differential

nicotine-induced target effects were observed following the 12–30 hpf exposure window. In those zebrafish, the ventral and mediolateral SMN axons projected normally, but the dorsal SMN axons did not (Table 1). These findings suggest that dorsal projecting SMN axons are more susceptible to nicotine exposure than ventral and mediolateral projecting SMN axons. It also suggests that different mechanisms possibly underlie the actions of nicotine. Consequently, we focused our analysis on the dorsal projecting SMN axons regardless of the nature of the pathfinding error (Fig. 4A). It became clear that the percent of dorsal projecting SMN axons with abnormal pathfinding phenotypes was increased for all nicotine concentrations between 22–72 hpf (Fig. 4B; one-way ANOVA, $F_{(4,43)} = 60.494$, $p < 0.001$, Holm-Sidak *post hoc* test). However, if embryos were exposed from 12–30 hpf, abnormal SMN axonal phenotypes only occurred at high nicotine concentrations (15 and 30μM; Fig. 4B, Kruskal-Wallis one-way ANOVA on ranks, $H_{(4)} = 16.859$; p=0.002, Dunn's *post hoc*).

Nicotine-induced pathfinding phenotypes of dorsal projecting secondary motoneuron axons

In order to better understand the differential effects of nicotine exposure on SMN axonal pathfinding, the dorsal projecting SMN axon pathfinding errors were categorized based on the nature of their phenotype. Four phenotypically distinct, nicotine-induced axonal pathfinding errors emerged which describe deficits in SMN axon pathfinding and myotomal targeting (Fig. 5). The first of the abnormal phenotypes was characterized by distinct errors in axon trajectory. Dorsal projecting axons that belong in this group appear to successfully reach their dorsal-most targets in the periphery. However, in some cases as they exit the spinal cord they fail to turn dorsally at the appropriate intermediate turning point (Fig. 5B, arrowheads; compare to control in Fig. 5A right panel). Instead, they often extended far caudally past that point before turning dorsally. In other cases, the dorsal projecting axon exhibited very distinct sharp turns (Fig. 5B, arrows) as they navigated within the myotome. Therefore, if SMN axons exhibited any of the aforementioned errors, they were classified as having "trajectory" errors.

The second phenotypically distinct SMN axonal pathfinding error describes dorsal projecting SMN axons that exhibited a "fork"-like (split) phenotype as they projected into the dorsal myotome (Fig. 5C, filled arrows). In these cases, a subset of axons separated from the main dorsal SMN nerve bundle and extended in different directions. This resulted in the axons splitting along two different paths which yielded the "split" axon phenotype.

The third distinct pathfinding error caused by nicotine exposure was the "stall" axon error. This phenotype was characterized by dorsal projecting axons that stalled at the turning point and then failed to fully reach the dorsal periphery (Fig. 5D, circle). In some cases, even though it was evident that the dorsal projecting axons stalled at the ventral root (Fig. 5D), a subset of dorsal projecting axons could be detected, and appeared as very thin fibers (Fig. 5D, arrowheads).

Following this careful description of dorsal SMN axon phenotypes caused by nicotine exposures, we specifically examined dorsal projecting axons according to phenotypically distinct errors. We found that the "trajectory" error phenotypes occurred at all nicotine concentrations between 22–72 hpf (Fig 6A; one-way ANOVA, $F_{(4,43)} = 23.755$, $p < 0.001$,

Holm-Sidak *post hoc* test), whereas when exposed between 12–30 hpf only high concentrations of nicotine (15 and 30μM) affected dorsal SMN axons (Fig. 6A; one-way ANOVA, $F_{(4,25)} = 5.044$, $p = 0.004$, Holm-Sidak *post hoc* test). Also, dorsal projecting axons in fish exposed between 22–72 hpf exhibited the "split" error phenotype predominately at 5 and 15μM nicotine exposure (Fig. 6B; Kruskal-Wallis one-way ANOVA on ranks, $H_{(4)} = 27.406$; $p<0.001$, Dunn's *post hoc*). However, the "stall" axon phenotype mostly occurred in fish exposed to 30μM nicotine and less when exposed to 1 and 15μM nicotine from 22–72 hpf (Fig. 6C; Kruskal-Wallis one-way ANOVA on ranks, $H_{(4)} = 29.627$; $p<0.001$, Dunn's *post hoc*). Taken together, these results indicate that a 1μM nicotine exposure from 22–72 hpf as well as 15 and 30μM nicotine from 12–30 hpf primarily cause "trajectory" errors.

Lastly, a fourth phenotypically distinct pathfinding error caused by nicotine exposure, which could not easily fit into the other 3 categories, was the duplication of SMN ventral projecting nerve bundles within a hemisegment (Supplemental Fig. 2A and B). Even though these duplicated axons projected ventrally, they were confined within the dorsal myotome and did not extend their axons beyond the midline into the ventral myotome. This phenotype occurred more frequently in 30μM nicotine-exposed zebrafish and was only evident when the exposure window was from 22–72 hpf (Supplemental Fig. 2B).

A subset of primary motoneurons can be visualized using the β2 nAChR antibody

We have presented four distinct SMN axonal phenotypes in larval zebrafish caused by embryonic nicotine exposure. Specifically, the "trajectory" errors in SMN axons occur in approximately 50% of the segments analyzed when exposed to nicotine between 22–72 hpf at low concentrations (1μM). Similar errors occurred when embryos were exposed at higher concentrations of nicotine (15 and 30μM) between 12–30 hpf and then analyzed at 72 hpf. Interestingly, during the shorter and earlier exposure window (12–30 hpf) nicotine was withdrawn prior to most SMN axons exiting the spinal cord and extending in the dorsal myotome. Therefore, we hypothesized that nicotine may affect earlier born dorsal projecting motoneurons that undergo axon extension during this early time window. It was previously shown that primary motoneurons are among the earliest born and their axonal trajectory paths are used by SMNs as a guide at later stages (Pike et al., 1992). We asked then whether nicotine exposure affected the dorsal projecting primary motoneuron axon (MiP, Middle Primary), which could then influence dorsal projecting SMN axons and thus manifest as "trajectory" errors when visualized using the zn5 antibody.

In order to test this possibility, we used an antibody (*anti-chrn2b*) designed to target β_2 nAChR subunits in a previous study (Welsh et al. 2009) to specifically label the dorsally projecting PMN axon. In that study, the β_2 nAChR subunit was detected on zebrafish Rohon-Beard neurons and motoneuron axons. In the current study, we used a series of immunolabeling experiments to demonstrate that this antibody labels a subset of PMNs; specifically the CaP (Caudal Primary) and MiP (Middle Primary) motoneuron somata and axons (Fig. 7, n= 177 embryos and larvae, Supplement Table 1). Immunolabeling at 28 hpf with the β_2 nAChR antibody labels the CaP somata and its axon (Fig. 7A; open and filled arrows indicate the soma and axon, respectively) and by 30–32 hpf, a dorsal projecting axon

can be detected (Fig. 7B and C, yellow arrow). Occasionally, *anti-chrn2b* labeling detected large cell bodies adjacent to CaP somata which were likely presumptive MiP cell bodies (Fig. 7C, yellow circle).

Dual immunostaining at 28 hpf with *anti-chrn2b* along with the znp-1 antibody which is primarily used to label PMN axons, revealed co-labeling on the same ventrally projecting axon (CaP axon) (Fig. 7D, E). However, co-staining at 31 hpf with *anti-chrn2b* and the zn5 antibody which labels SMN axons (Fig. 7F) revealed two non-overlapping ventrally projecting axons. These expression profiles suggest that *anti-chrn2b* labels the zn5-negative, CaP axon. At timepoints between 31 and 36 hpf, the same dorsally projecting axon was co-labeled with the znp-1 antibody and *anti-chrn2b* (Fig. 7G–I; Supplemental Fig. 3A–C). This suggested that this dorsally projecting, *anti-chrn2b* positive axon, at these early developmental stages was most likely the MiP axon.

To further substantiate *anti-chrn2b* labeling of the MiP axon, we performed *anti-chrn2b* immunostaining in *parg*^{mn2Et} zebrafish, which express green fluorescent protein (GFP) in motoneurons early in embryogenesis (Balciunas et al., 2004). At 24 hpf, GFP-positive MiP axons in *parg*^{mn2Et} are readily detected (Fig. 7J, white arrows). This was true for 28 hpf, 32 hpf, and 36 hpf embryos (data not shown). When 34 hpf *parg*^{mn2Et} embryos (Fig. 7K–M) were labeled with *anti-chrn2b*, the putative MiP axons (Fig. 7K and 7L) as well as the CaP axons (not shown) were labeled. These experiments using *parg*^{mn2Et} embryos validated the results from the labeling studies using znp-1 and *anti-chrn2b*. The *anti-chrn2b* antibody is most likely labeling both CaP and MiP axons which would be a useful tool to facilitate dual labeling studies in the same embryo/larva to simultaneously examine nicotine effects on PMN axons (*anti-chrn2b* labeling) along with SMN axons (zn5 labeling).

In order to use the *anti-chrn2b* to label putative PMN axons, we first confirmed that even at later developmental time points (36–72 hpf), the *anti-chrn2b* labeling was still robust (Supplemental Fig. 3A–C for 36 hpf embryo) and was confined to PMN axons. In 48-hpf embryos, the znp1-positive, main ventral projecting axon, still appeared to colocalize directly with the *anti-chrn2b* signal (not shown). However, dual labeling with the zn5 antibody and *anti-chrn2b* revealed no apparent colocalization of the two markers on a single ventral projecting motor axon (Supplemental Fig. 3D–E). Moreover, at 48 hpf, the dorsal projecting, zn5-positive SMN axons still have not projected to the periphery, but *anti-chrn2b* is clearly detecting a dorsal projecting axon at this stage; which is likely the MiP axon. In the transgenic zebrafish line, Tg(*gata2*:GFP), which express GFP in ventral projecting SMN axons, *anti-chrn2b* did not label the ventral projecting, GFP-positive SMN axon (Supplemental Fig. 3F).

By 72 hpf, the zn5-positive dorsal projecting SMN axons can now be easily detected in the periphery. These axons did not appear to colocalize with the *anti-chrn2b*-positive axon (likely MiP; denoted by white circle in Supplemental Fig. 3G) in the dorsal periphery, as there is a clear separation between the labeled axons. However, as the zn5-positive axons first exited spinal cord, they appeared to overlap tightly with the *anti-chrn2b* positive MiP axon (Supplemental Fig. 3G, white arrow).

Uncoupling nicotine-induced pathfinding errors in primary and secondary motoneuron axons

Double labeling studies were performed in embryos exposed to nicotine using the same exposure windows and concentrations presented earlier in this study (n=116, Supplement Table 1). Immunolabeling with zn5 and *anti-chrn2b* at 72 hpf in control larva shows that the dorsal zn5-positive SMN axons take the same trajectory to the periphery as the *chrn2b*-positive MiP axon (Fig. 8A–C). Based on the dose response and exposure window for nicotine, the SMN "trajectory" errors could be replicated by using high nicotine concentrations (30μM, Fig. 8D–F) between 12–30 hpf as well as low (1μM, Fig. 8G–I) or high (30μM, Fig. 8J–L) nicotine concentrations between 22–72 hpf. These larvae exhibited SMN axonal trajectory errors as denoted by the yellow arrows (see Fig. 8D, G and J) and were accompanied by errors in the *anti-chrn2b* positive MiP-like axon. Whenever a true "trajectory" error was present in SMN axons (yellow arrows in figure 8), the corresponding PMN axons exhibited the same trajectory error regardless of the window of exposure or concentration of nicotine.

We then determined if any of the other nicotine-induced SMN axonal phenotypes were potentially linked to altered PMN axon morphology as it appeared that SMN axons were following the lead of PMN axons as they exited spinal cord and entered the periphery. When SMN axons were stalled entering the periphery (Fig. 9A, yellow arrows), PMN axons were still observed to extend well into the periphery; they did not retract (Fig. 9B–C). The nicotine-induced duplication of SMN axon nerve roots (Fig. 9D, yellow arrow) was observed in segments where ventral projecting PMN axons clearly were not duplicated (Fig. 9E). In fact, duplicated PMN axons have not been observed in any of our nicotine studies.

Interestingly, in some segments, the SMN nerve bundle appeared to stall but seemed to have a single axon that was navigating into the dorsal periphery. This single SMN axon still appeared to use the *anti-chrn2b*-positive PMN axon (MiP) as a guide. In this case, the PMN axon appeared to properly orientate the SMN axon towards the dorsal periphery (Fig. 10A–C; magnified views shown in Fig. 10D–F). Thus, consistent with data shown in figure 9, the putative MiP axon was acting as a guide for dorsal projecting SMN axons especially when in proximity to the ventral nerve exit point (Fig. 10A, D, asterisk). However, once SMN axons navigated distally in the dorsal periphery (Fig. 10I, yellow arrow), the nicotine-induced errors could occur independent of the corresponding PMN axon. (Fig. 10I, white arrow). Lastly, when SMN axons had a "split" axon error within the dorsal periphery, the corresponding PMN axon within that segment did not appear to have branches extending from it that would influence the SMN axons causing them to take "wrong" directions to the periphery (not shown).

Discussion

In this study, we show that motoneuron axon pathfinding errors and muscle degeneration in zebrafish depend on the concentration of nicotine, along with the length and developmental window of the exposure. We demonstrate that nicotine exposure not only can affect axons of different motoneuron subtypes but can also differentially influence axons within a given motoneuron subtype that projects either dorsally, ventrally or mediolaterally into the muscle.

We also reveal that nicotine can differentially affect muscle morphology which could potentially influence motor axon pathfinding. Additionally, we show that nicotine exposure can lead to morphologically distinct phenotypes for dorsal projecting motoneuron axons. These results highlight the potentially intricate actions of nicotine and provide needed insight for understanding potential mechanisms underlying nicotine-induced axonal pathfinding errors.

Uncoupling axonal pathfinding errors and muscle degeneration

In zebrafish, primary and secondary motoneurons extend their axons in a stereotypical manner to reach their appropriate target muscles. They navigate into the periphery with remarkable precision and any alterations in the intrinsic or extrinsic factors that help guide them, can lead to pathfinding errors. The earliest born motoneurons (PMNs) in zebrafish begin extending their axons in the myotome at ~16–17 hpf and make functional contacts with the slow muscle fibers around that time; at ~24 hpf SMN emerge and follow the PMNs (Myers et al., 1986; Eisen et al., 1986; Jackson and Ingham, 2013). Muscle fibers possess nicotinic acetylcholine receptors which makes them susceptible to nicotinic insult. Therefore, when investigating the neuronal effects of nicotine in a whole developing system, it is important to account for potential nicotine-induced effects on muscle fiber morphology (Welsh et al., 2009). In this study, we show that nicotine-induced axonal pathfinding errors can occur in the presence or absence of muscle defects depending on the concentration of nicotine and the window of exposure. When wildtype zebrafish were exposed from 22–72 hpf to 15 and 30μM nicotine, axonal pathfinding abnormalities and muscle degeneration occurred concurrently. However, when zebrafish were exposed to lower concentrations of nicotine (1 and 5μM, 22–72 hpf), abnormalities in axonal targeting were present even in the absence of quantifiable muscle defects.

Since the axonal pathfinding errors appeared to be far more robust at nicotine concentrations that also caused muscle degeneration, it is possible that muscle defects could influence motoneuron axon pathfinding. It is widely accepted that nerve-muscle interactions are important for proper axon growth and target selection (Funakoshi et al., 1995). In zebrafish, proper migration and guidance of spinal motor axons are dependent upon certain muscle-derived cues (Feldner et al., 2005; Schweitzer et al., 2005; Schneider and Granato, 2006). Nicotine-induced abnormalities in muscle morphology may impair the ability of the muscle to provide the appropriate cues back to the spinal motor axons. In this scenario, the axons would either be misrouted to inappropriate targets or potentially stalled at intermediate target points (Knobel et al., 1999).

Notably, zebrafish embryos exposed to nicotine from 12–30 hpf did not exhibit slow muscle degeneration at nicotine concentrations that usually resulted in muscle morphology defects when exposed between 22–72 hpf. The transcript for the zebrafish muscle receptor β1 subunit has been shown to be robustly unregulated between 48–72 hpf (Papke et al., 2012). Such differences in the level of muscle nicotinic receptor expression could account for the differential effects of nicotine on muscle fibers at different stages of development. Hence, when exposed from 12–30 hpf, the nicotine effects on muscle may be minimal even at high concentrations of nicotine due to the inherently low levels of functional muscle receptors.

However, if the nicotine exposure largely overlaps with the increase in muscle receptor levels (22–72 hpf exposure window), this could result in receptor over-activation and thus muscle degeneration. Alternatively, compensatory mechanisms may also account for the lack of muscle defects when embryos were exposed from 12–30 hpf. Embryos were removed from nicotine at 30 hpf which may have allowed any affected slow muscle fibers to recover and exhibit normal muscle morphology by 72 hpf. Taken together, these results suggest that nicotine can potentially influence neuronal and muscle effects independently. In the absence of muscle effects, the nicotine-induced SMN axonal targeting errors appeared more subtle, but were still evident providing further support for the neural specific actions of nicotine (Svoboda et al, 2002).

Nicotine-induced effects on dorsal, ventral, and mediolateral projecting SMN axons

Nicotine-induced motoneuron axon pathfinding errors were mostly associated with the dorsal projecting axons rather than the ventral and mediolateral projecting ones. Ablation experiments in zebrafish have shown that in the absence of ventral primary motoneurons (CaP), SMN extend their axons properly and reach their targets (Pike et al., 1992). However, in the absence of the MiP motoneurons, dorsal projecting SMN axons often extend into the periphery along incorrect paths. Importantly, SMN axons exit the spinal cord in a sequential manner. First, ventral SMNs extend their axons, followed by the mediolateral projecting SMN axons and lastly by the dorsal projecting axons (Ott et al., 2001). Such differences in the timing of axon extension could contribute to errors seen mainly on dorsal projecting axons following the different nicotine exposure windows. Therefore, each nicotine exposure in combination with the levels of nicotine may exert differential effects depending on when SMN axons have already exited the spinal cord. Moreover, motoneurons that project axons dorsally, express different transcription factors compared to those motoneurons that have ventrally projecting axons, enabling them to use distinct signaling cues and pathways for axon extension and targeting (Guthrie, 2007; Sharma et al., 2000). This differential ability of dorsal, ventral, and mediolateral SMN axons to establish their normal pathways suggests that different guidance cues govern path choice. Consequently, nicotine exposure could alter signaling pathways and guidance cues specifically required for dorsal projecting SMN axons to make correct path choices.

It is known that nicotine can directly act upon presynaptic nAChRs and affect motoneuron axon branching via presynaptic mechanisms (An et al., 2010). Even though the developmental expression profile of nAChR subunits has been described in zebrafish (Zirger et al., 2003; Ackerman et al., 2009; Menelaou et al., 2014), the exact spatiotemporal and combinatorial profile of nAChRs still remains unknown. nAChRs are assembled in a wide range of subunit combinations and they exhibit differences in Ca^{+2} permeability, channel kinetics, desensitization rate and agonist/antagonist sensitivity (Kalamida et al., 2007). Interestingly, nicotine has been shown to be most potent and efficacious in activating the zebrafish α4β2 receptor subtype as compared to other heteromeric β2-containing nAChR subtypes, when expressed and analyzed in *Xenopus* oocytes (Papke et al., 2012). Thus, it is possible that the localization of different of nAChR subtypes to dorsal, ventral or mediolateral SMN axons can directly influence nicotine's ability to alter SMN axonal pathfinding; with some axons being more severely affected than others.

Possible mechanisms underlying nicotine-induced motoneuron axon phenotypes

The differential effects of nicotine on motoneuron axons indicate that the actions of nicotine are multifaceted. One possible explanation for the nicotine-induced effects observed in SMN axons could be due to alterations of calcium homeostasis, which can then inappropriately affect downstream Ca^{2+}-mediated signaling pathways critical in the expression of intrinsic molecules. The frequency and strength of Ca^{2+} transients has been shown to effectively modulate gene activity and differentially activate signaling pathways (Dolmetsch et al., 1997; Greer and Greenberg, 2008). Therefore, inappropriate nicotine-induced activation of nAChRs at critical developmental stages may disrupt the normal course of gene expression, thus disrupting the expression profiles of axon pathfinding-specific molecules. Another possible mechanism may involve altering muscle-derived or environmental cues important for axon pathfinding.

The motoneuron axonal “trajectory” errors were among the most commonly observed axon pathfinding errors following nicotine exposures (12–30 hpf and 22–72 hpf). Even though these trajectory errors occurred at all nicotine concentrations when exposed between 22–72 hpf, that was not the case for the short exposure window. Given that the trajectory errors were still likely to occur at concentrations that muscle morphology was not affected, we argue that the “trajectory” errors could potentially be caused by nicotine independent of muscle defects. In this context, there are at least two possible mechanisms that could produce the trajectory errors observed in zebrafish upon nicotine exposure. First, altering the frequency of rhythmic bursting activity during motoneuron axon outgrowth can result in pathfinding errors (Hanson and Landmesser, 2004, 2006). Zebrafish embryos exhibit robust spontaneous activity between 17–28 hpf (Saint-Amant and Drapeau, 1998, Thomas et al., 2009). This intrinsic spontaneous activity is associated with Ca^{2+} transients in the motoneuron soma and growth cones (Plazas et al., 2013; Hanson and Landmesser, 2003) and results in the activation of muscle nicotinic receptors by the release of acetylcholine (Wang et al., 2009). We also know that transient nicotine exposure dramatically increases the embryonic motor activity in zebrafish (Thomas et al., 2009). Therefore, nicotine application during motoneuron development and axon outgrowth can alter the frequency of the motoneuron bursting activity through activation of spinal nAChRs, and potentially disrupt motor axon pathfinding decisions in zebrafish.

Alteration of calcium homeostasis can potentially affect both primary and secondary motoneurons. Therefore, an alternative mechanism underlying the “trajectory” errors could involve nicotine-induced alterations of PMN axons that extend first even before SMNs start extending their axons into the periphery. This would subsequently result in the abnormal pathfinding of SMN axons. In zebrafish, it is known that secondary motoneurons extend their axons following a path previously established by primary motoneurons (Pike et al., 1992). In some of the experiments reported here, zebrafish embryos were exposed to nicotine before the dorsal projecting primary motoneuron (MiP) axons start to extend in the dorsal myotome. If nicotine exposure altered the normal trajectory of MiP axons, this could influence SMN axon pathfinding. For example, SMN dorsal projecting axons could follow the incorrect path set by MiP axons and at 72 hpf, this would be detected as a “trajectory” error. Our examination of PMN and SMN axons in the same fish using the *anti-chrn2b*

antibody revealed that these nicotine-induced “trajectory” errors were also present in PMNs, specifically the MiP axon. As MiP axons exited the spinal cord they drifted further caudal than they would normally do, SMNs appeared to follow the same PMN axon tract as they exited spinal cord. It appeared that whatever trajectory the MiP axons took when initially exiting spinal cord, the SMN axon would use it as a guide and such phenotypes appeared similar to those observed in *sidetracked* mutants where plexin A3 signaling is compromised (Palaisa and Granato, 2007).

The nicotine-induced “split” error phenotype was most commonly observed in zebrafish when exposed to 5 and 15μM nicotine (22–72 hpf window of exposure), but it was sparsely seen in fish exposed from 12–30 hpf. The distinction of this phenotype from the “trajectory” errors was the single point bifurcation (split) along the dorsal axon. Similar bifurcation behavior of motor axons has been reported for the ventrally projecting primary motoneuron axon (CaP) (Sainath and Granato, 2013). In that study, the intrinsic expression of plexin A3 receptors and an unidentifiable extrinsic cue known as turnout, played important roles in the proper and well-timed bifurcation in addition to maintaining the stability of branch points for CaP axon. Plexin A3 and turnout are intrinsic and extrinsic cues, respectively, both shown to be associated with the ventral CaP axon. If either of them, or some other similar cues were affected by nicotine exposure, this would in turn lead to premature axon splitting and potentially aberrant branching of dorsal SMN axons.

Following a nicotine exposure paradigm which was associated with muscle degeneration (30μM, 22–72 hpf), there was a higher likelihood to observe motoneurons with stalled axons at the spinal cord exit point. It is known that axon retraction and growth cone stalling are also associated with high frequency Ca^{2+} transients. When axons stall at intermediate decision points, they exhibit a high frequency of Ca^{2+} transients and when they begin to turn and elongate towards their target, Ca^{2+} transients are abolished (Gomez and Spitzer, 1999). Upon nicotine exposure, activation of neuronal and muscle AChRs occurs. This over-activation of nAChRs during critical periods of axon growth can result in high frequency Ca^{2+} transients, thus leading to axon stalling. In chick ciliary ganglion neurons, activation of α-bungarotoxin-sensitive nAChRs by nicotine exposure causes neurite retraction and inhibits neurite extension in a calcium-dependent manner (Pugh and Berg, 1994). In zebrafish, PMN axons can stall during pathfinding if they lack the *stumpy* gene. With this mutation, PMN axons do not receive the attracting signals from the periphery and this prevents them from extending beyond their intermediate targets (Beattie et al., 2000). This suggests that altering the frequency of intracellular Ca^{2+} transients along with changes in the muscle-derived cues from the environment (due to muscle degeneration possibly) play critical roles in proper axonal extension. However, in the *stumpy* mutants, only PMN axons were analyzed (Beattie et al., 2000), therefore it was not clear whether SMN axons also exhibited similar phenotypes. In this study, dorsal-projecting SMN axons were stalled even though their corresponding MiP motoneurons had extended their axon into the periphery. The nicotine-induced “stall” errors typically occurred at concentrations and exposure windows that also caused muscle degeneration. Interestingly, the muscle degeneration did not appear to overtly affect PMN axon targeting or morphology which suggests that muscle-derived cues may not substantially influence PMN axonal targeting to the periphery.

The presence of duplicated ventral projecting motor axons appearing as additional exit points in the dorsal myotome is not unique to the nicotine exposure paradigms reported here. In zebrafish, blocking the expression of neuropilin-1 and plexin A3, two receptors that bind axon-repelling semaphorins, induces additional exit points of spinal motor nerves from spinal cord (Feldner et al., 2005; Palaisa and Granato, 2007). These axon duplications mainly occurred within the posterior end of the somite, where semaphorins are highly concentrated thus restricting the extension of spinal motor axons in the anterior part of the somite. Therefore, if motoneuron axons fail to express axon-repellent receptors, they would be unable to detect signals that would normally restrict them from entering the posterior end of the somite. In those studies, the primary focus was on PMN axon pathfinding. In our experiments, we were able to analyze both PMN and SMN axons in the same fish and found that nicotine exposure could result in SMN axons being duplicated when PMN axons in the same segment were not. Thus, the exposure was likely directly affecting SMN axons and likely affecting signaling mechanisms other than plexin A3 or the semaphorins.

In summary, embryonic nicotine exposure can affect cholinergic signaling and consequently lead to motoneuron axon pathfinding errors of spatially distinct axonal trajectories in zebrafish. Different types of motoneurons (PMNs and SMNs) exhibited phenotypically distinct axonal alterations following exposure to nicotine and the mechanisms underlying the nicotine-induced effects most likely involve complex intrinsic and extrinsic pathways. However, the specific mechanisms underlying the actions of nicotine on neural and muscle substrates is unclear and still remains to be examined in the future.

Supplementary Material

Refer to Web version on PubMed Central for supplementary material.

Acknowledgements

This work was supported by the National Institute of Health (NIH)/National Institute of Environmental Health Sciences (NIEHS), Grant Number ES016513 to KRS and NIEHS Grant number 2P30ES004184. We thank Robin Grisaffe for expert fish care. We also thank Madelyn Weil for helping with the dual fluorescent labeling and imaging experiments. We thank Dr. Stephen Ekker for providing our research group with the *parg*^{mn2Et} enhancer trap line of zebrafish.

Abbreviations

hpf	hours post fertilization
CaP	Caudal Primary
MiP	Mid Primary
PMN	primary motoneuron
SMN	secondary motoneuron
GFP	green fluorescent protein
nAChR	nicotinic acetylcholine receptor

References

Ackerman KM, Nakkula R, Zirger JM, Beattie CE, Boyd RT. Cloning and spatiotemporal expression of zebrafish neuronal nicotinic acetylcholine receptor alpha 6 and alpha 4 subunit RNAs. Dev Dyn. 2009; 238(4):980–992. [PubMed: 19301390]

An MC, Lin W, Yang J, Dominguez B, Padgett D, Sugiura Y, Aryal P, Gould TW, Oppenheim RW, Hester ME, Kaspar BK, Ko C, Lee K. Acetylcholine negatively regulates development of the neuromuscular junction through distinct cellular mechanisms. PNAS. 2010; 107(23):10702–10707. [PubMed: 20498043]

Balciunas D, Davidson AE, Sivasubbu S, Hermanson SB, Welle Z, Ekker SC. Enhancer trapping in zebrafish using the Sleeping Beauty transposon. BMC Genomics. 2004; 5:62. [PubMed: 15347431]

Beattie CE, Melancon E, Eisen JS. Mutations in the stumpy gene reveal intermediate targets for zebrafish motor axons. Development. 2000; 127(12):2653–2662. [PubMed: 10821763]

Behra M, Cousin X, Bertrand C, Vonesch JL, Biellmann D, Chatonnet A, et al. Acetylcholinesterase is required for neuronal and muscular development in the zebrafish embryo. Nature Neuroscience. 2002; 5(2):111–118. [PubMed: 11753420]

Brennan C, Mangoli M, Dyer CE, Ashworth R. Acetylcholine and calcium signalling regulates muscle fibre formation in the zebrafish embryo. J Cell Sci. 2005; 118(Pt 22):5181–5190. [PubMed: 16249237]

Devoto SH, Melancon E, Eisen JS, Westerfield M. Identification of separate slow and fast muscle precursor cells in vivo, prior to somite formation. Development. 1996; 122(11):3371–3380. [PubMed: 8951054]

Dolmetsch RE, Lewis RS, Goodnow CC, Healy JI. Differential activation of transcription factors induced by Ca2+ response amplitude and duration. Nature. 1997; 386(6627):855–858. [PubMed: 9126747]

Eisen JS, Myers PZ, Westerfield M. Pathway selection by growth cones of identified motoneurones in live zebra fish embryos. Nature. 1986; 320:269–271. [PubMed: 3960108]

Engel AG, Lambert EH, Mulder DM, Torres CF, Sahashi K, Bertorini TE, et al. A newly recognized congenital myasthenic syndrome attributed to a prolonged open time of the acetylcholine-induced ion channel. Ann Neurol. 1982; 11(6):553–569. [PubMed: 6287911]

Fashena D, Westerfield M. Secondary motoneuron axons localize DM-GRASP on their fasciculated segments. Journal of Comparative Neurology. 1999; 406(3):415–424. [PubMed: 10102505]

Feldner JBT, Goishi K, Schweitzer J, Lee P, Schachner M, Klagsbrun M, Becker CG. Neuropilin-1a is involved in trunk motor axon outgrowth in embryonic zebrafish. Dev Dyn. 2005; 234(3):19.

Funakoshi H, Belluardo N, Arenas E, Yamamoto Y, Casabona A, Persson H, et al. Muscle-Derived Neurotrophin-4 as an Activity-Dependent Trophic Signal for Adult Motor-Neurons. Science. 1995; 268(5216):1495–1499. [PubMed: 7770776]

Gomez CM, Maselli RA, Groshong J, Zayas R, Wollmann RL, Cens T, et al. Active calcium accumulation underlies severe weakness in a panel of mice with slow-channel syndrome. J Neurosci. 2002; 22(15):6447–6457. [PubMed: 12151524]

Gomez TM, Spitzer NC. In vivo regulation of axon extension and pathfinding by growth-cone calcium transients. Nature. 1999; 397(6717):350–355. [PubMed: 9950427]

Greer PL, Greenberg ME. From synapse to nucleus: calcium-dependent gene transcription in the control of synapse development and function. Neuron. 2008; 59(6):846–860. [PubMed: 18817726]

Guthrie S. Patterning and axon guidance of cranial motor neurons. Nat Rev Neurosci. 2007; 8(11): 859–871. [PubMed: 17948031]

Hanson MG, Landmesser LT. Characterization of the circuits that generate spontaneous episodes of activity in the early embryonic mouse spinal cord. Journal of Neuroscience. 2003; 23(2):587–600. [PubMed: 12533619]

Hanson MG, Landmesser LT. Normal patterns of spontaneous activity are required for correct motor axon guidance and the expression of specific guidance molecules. Neuron. 2004; 43(5):687–701. [PubMed: 15339650]

Hanson MG, Landmesser LT. Increasing the frequency of spontaneous rhythmic activity disrupts pool-specific axon fasciculation and pathfinding of embryonic spinal motoneurons. J Neurosci. 2006; 26(49):12769–12780. [PubMed: 17151280]

Jackson HE, Ingham PW. Control of muscle fibre-type diversity during embryonic development: the zebrafish paradigm. Mech Dev. 2013; 30(9–10):447–457. [PubMed: 23811405]

Kalamida D, Poulas K, Avramopoulou V, Fostieri E, Lagoumintzis G, Lazaridis K, Sideri A, Zouridakis M, Tzartos SJ. Muscle and neuronal nicotinic acetylcholine receptors. FEBS J. 2007; 274(15):3799–3845. [PubMed: 17651090]

Knobel KM, Jorgensen EM, Bastiani MJ. Growth cones stall and collapse during axon outgrowth in Caenorhabditis elegans. Development. 1999; 126(20):4489–4498. [PubMed: 10498684]

Lefebvre JL, Ono F, Puglielli C, Seidner G, Franzini-Armstrong C, Brehm P, et al. Increased neuromuscular activity causes axonal defects and muscular degeneration. Development. 2004; 131(11):2605–2618. [PubMed: 15128655]

Menelaou E, McLean DL. A gradient in endogenous rhythmicity and oscillatory drive matches recruitment order in an axial motor pool. J Neurosci. 2012; 32(32):10925–10939. [PubMed: 22875927]

Menelaou E, Svoboda KR. Secondary motoneurons in juvenile and adult zebrafish: axonal pathfinding errors caused by embryonic nicotine exposure. J Comp Neurol. 2009; 512(3):305–322. [PubMed: 19006183]

Menelaou E, Udvadia AJ, Tanguay RL, Svoboda KR. Activation of α2A-containing nicotinic acetylcholine receptors mediates nicotine-induced motor output in embryonic zebrafish. Eur J Neurosci. 2014; 40(1):2225–2240. [PubMed: 24738729]

Myers PZ, Eisen JS, Westerfield M. Development and axonal outgrowth of identified motoneurons in the zebrafish. J Neurosci. 1986; (8):2278–2289. [PubMed: 3746410]

Ono F, Higashijima S, Shcherbatko A, Fetcho JR, Brehm P. Paralytic zebrafish lacking acetylcholine receptors fail to localize rapsyn clusters to the synapse. J Neurosci. 2001; 21(15):5439–5448. [PubMed: 11466415]

Ott H, Diekmann H, Stuermer CA, Bastmeyer M. Function of Neurolin (DM-GRASP/SC-1) in guidance of motor axons during zebrafish development. Dev Biol. 2001; 235(1):86–97. [PubMed: 11412029]

Palaisa KA, Granato M. Analysis of zebrafish sidetracked mutants reveals a novel role for Plexin A3 in intraspinal motor axon guidance. Development. 2007; 134(18):3251–3257. [PubMed: 17699603]

Papke RL, Ono F, Stokes C, Urban JM, Boyd RT. The nicotinic acetylcholine receptors of zebrafish and an evaluation of pharmacological tools used for their study. Biochem Pharmacol. 2012; 84(3): 352–365. [PubMed: 22580045]

Plazas P, Nicol X, Spitzer NC. Activity-dependent competition regulates motor neuron axon pathfinding via PlexinA3. Proc Natl Acad Sci. 2013; 110(4):1524–1529. [PubMed: 23302694]

Pike SH, Melancon EF, Eisen JS. Pathfinding by zebrafish motoneurons in the absence of normal pioneer axons. Development. 1992; 114(4):825–831. [PubMed: 1618146]

Pugh PC, Berg DK. Neuronal Acetylcholine-Receptors That Bind Alpha-Bungarotoxin Mediate Neurite Retraction in a Calcium-Dependent Manner. Journal of Neuroscience. 1994; 14(2):889–896. [PubMed: 8301367]

Sainath R, Granato M. Plexin A3 and turnout regulate motor axonal branch morphogenesis in zebrafish. Plos One. 2013; 8(1):e54071. [PubMed: 23349787]

Saint-Amant L, Drapeau P. Time course of the development of motor behaviors in the zebrafish embryo. J Neurobiol. 1998; 37(4):622–632. [PubMed: 9858263]

Schneider VA, Granato M. The myotomal diwanka (lh3) glycosyltransferase and type XVIII collagen are critical for motor growth cone migration. Neuron. 2006; 50(5):683–695. [PubMed: 16731508]

Schweitzer J, Becker T, Lefebvre J, Granato M, Schachner M, Becker CG. Tenascin-C is involved in motor axon outgrowth in the trunk of developing zebrafish. Developmental Dynamics. 2005; 234(3):550–566. [PubMed: 16110513]

Sharma K, Leonard AE, Lettieri K, Pfaff SL. Genetic and epigenetic mechanisms contribute to motor neuron pathfinding. Nature. 2000; 406(6795):515–519. [PubMed: 10952312]

Svoboda KR, Linares AE, Ribera AB. Activity regulates programmed cell death of zebrafish Rohon-Beard neurons. Development. 2001; 128(18):3511–3520. [PubMed: 11566856]

Svoboda KR, Vijayaraghavan S, Tanguay RL. Nicotinic receptors mediate changes in spinal motoneuron development and axonal pathfinding in embryonic zebrafish exposed to nicotine. J Neurosci. 2002; 22(24):10731–10741. [PubMed: 12486166]

Thomas LT, Welsh L, Galvez F, Svoboda KR. Acute nicotine exposure and modulation of a spinal motor circuit in embryonic zebrafish. Toxicol Appl Pharmacol. 2009; 239(1):1–12. [PubMed: 19121331]

Wang S, Polo-Parada L, Landmesser LT. Characterization of rhythmic Ca2+ transients in early embryonic chick motoneurons: Ca2+ sources and effects of altered activation of transmitter receptors. J Neurosci. 2009; 29(48):15232–15244. [PubMed: 19955376]

Welsh L, Tanguay RL, Svoboda KR. Uncoupling nicotine mediated motoneuron axonal pathfinding errors and muscle degeneration in zebrafish. Toxicol Appl Pharmacol. 2009; 237(1):29–40. [PubMed: 18694773]

Westerfield M. The Zebrafish Book: A Guide for the Laboratory Use of Zebrafish (Danio Rerio). 1995

Zeller J, Granato M. The zebrafish diwanka gene controls an early step of motor growth cone migration. Development. 1999; 126(15):3461–3472. [PubMed: 10393124]

Zeller J, Schneider V, Malayaman S, Higashijima S, Okamoto H, Gui J, Lin S, Granato M. Migration of zebrafish spinal motor nerves into the periphery requires multiple myotome-derived cues. Dev Biol. 2002; 252(2):241–256. [PubMed: 12482713]

Zirger JM, Beattie CE, McKay DB, Boyd RT. Cloning and expression of zebrafish neuronal nicotinic acetylcholine receptors. Gene Expr Patterns. 2003; 3(6):747–754. [PubMed: 14643683]

Highlights

Embryonic nicotine exposure can specifically affect secondary motoneuron axons in a dose-dependent manner.

The nicotine-induced secondary motoneuron axonal pathfinding errors can occur independent of any muscle fiber alterations.

Nicotine exposure primarily affects dorsal projecting secondary motoneurons axons.

Nicotine-induced primary motoneuron axon pathfinding errors can influence secondary motoneuron axon morphology.

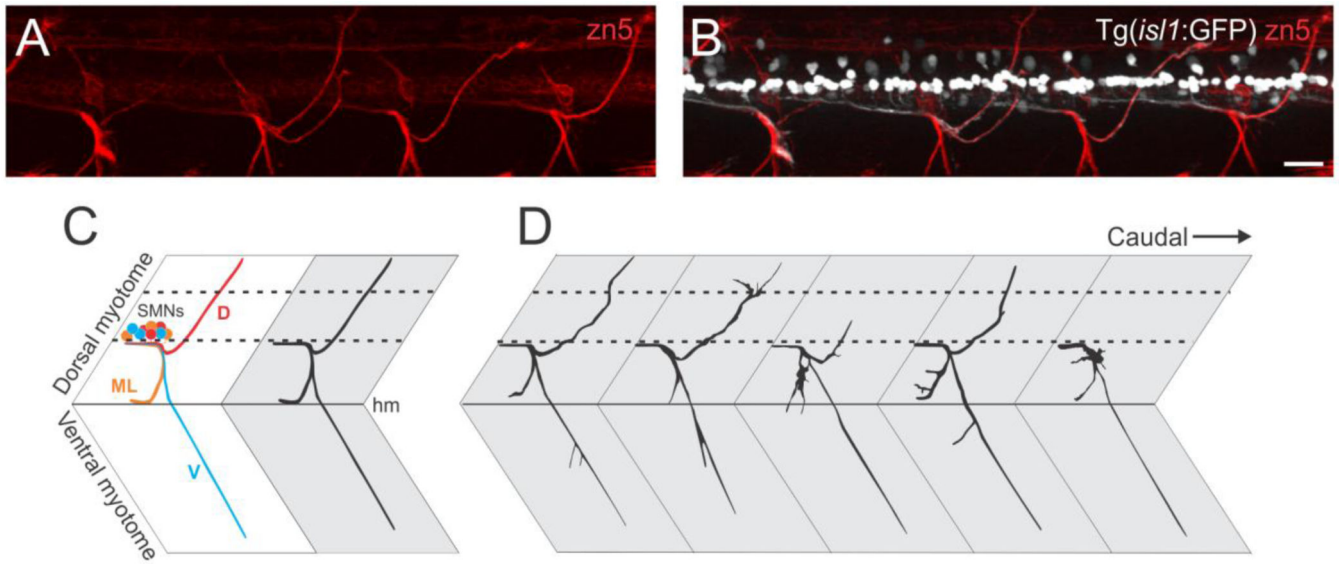

Figure 1. Secondary motoneuron axons and the effects of nicotine exposure on their axonal pathfinding

A) Photomicrograph of a 72-hpf larval Tg(*isl1*:GFP) zebrafish immunolabeled with the zn5 antibody (red) which specifically labels the main nerve of fasciculated SMNs axons. This zebrafish was exposed to nicotine (30μM) embryonically (22–72 hpf) and exhibits axonal pathfinding errors in 4 consecutive segments. B) zn5 immunostaining is shown in the Tg(*isl1*:GFP) larval zebrafish that expresses GFP (white) in a subset of secondary motoneurons (SMN). Zn5-positive axons colocalize with GFP-positive dorsal projecting SMN axons. C) Left segment shows a lateral view of different subpopulations of secondary motoneurons (SMNs, shown in orange, red and blue) located in ventral spinal cord (marked by dotted lines). Axons exit at mid-segmental root and extend dorsally (D, red), ventrally (V, blue), and mediolaterally (ML, orange). Right segment illustrates normal pathfinding of SMN axons as visualized by zn5 labeling. D) Examples of abnormal axonal pathfinding are shown in each segment in the dorsal and ventral myotome. Note that abnormal phenotypes can be seen for dorsal, ventral, and mediolateral projecting axons. Horizontal myoseptum: hm. Illustration is not drawn to scale. Scale bar, 20 μm.

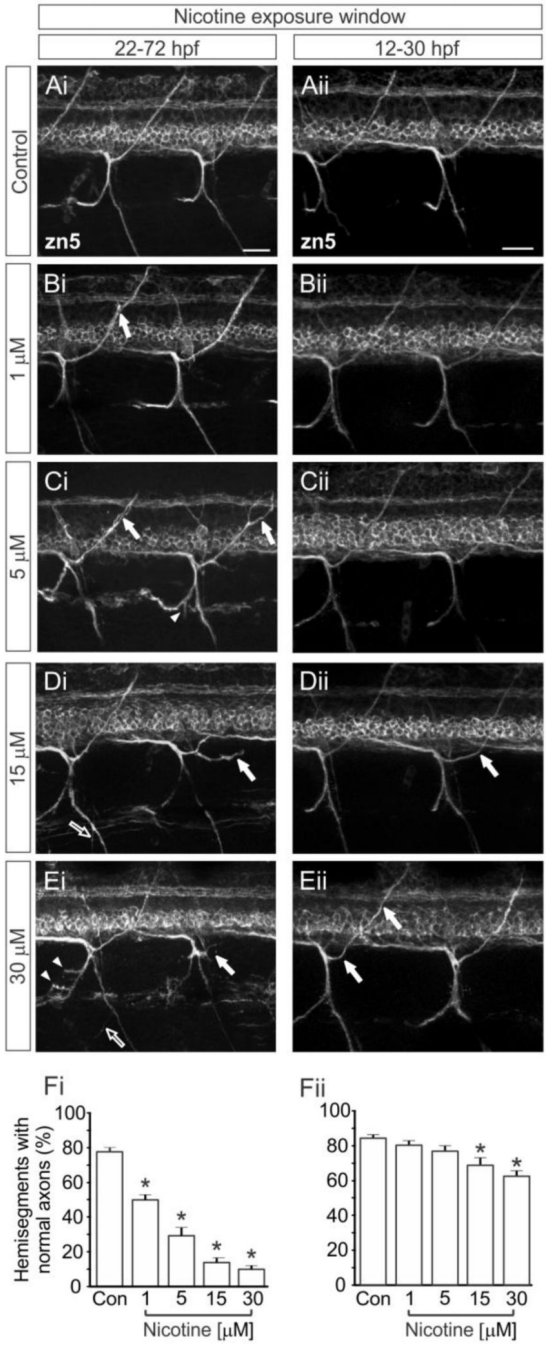

Figure 2. Nicotine-induced effects on SMN axons depend upon nicotine concentration and window of exposure

Ai) Zn5 immunoreactivity reveals SMN axons and their somata in 72-hpf control larva and corresponding zebrafish larvae exposed to varying concentrations of nicotine, 1μM (Bi), 5μM (Ci), 15μM (Di) and 30μM (Ei) from 22–72 hpf. Note the abnormal motoneuron axon trajectories in the nicotine-exposed zebrafish when compared to their control counterparts. Fi) At 72 hpf, the number of hemisegments with motoneuron axons that projected normally in the dorsal, ventral, and mediolateral myotomes over the total number of hemisegments analyzed in each fish was quantified and expressed as a percentage. Zebrafish exposed to

1μM (516 segments; 18 fish), 5μM (355 segments; 14 fish), 15μM (436 segments; 16 fish), and 30μM nicotine (359 segments; 14 fish) exhibited more hemisegments with abnormal motoneuron axon morphologies when compared to their stage-matched controls (455 segments; 17 fish). Asterisks in Fi denote statistical significance, p value < 0.001. Nicotine groups compared against the control using a *post hoc* Holm-Sidak test. Aii–Eii) Same as in Ai–Ei but for nicotine exposure window between 12–30 hpf. Fii) Quantification of nicotine-induced effects on SMN axons for exposure window 12–30 hpf. Zebrafish exposed to 1μM (176 segments; 7 fish) and 5μM nicotine (139 segments; 6 fish) were not significantly affected whereas when exposed at 15μM (125 segments; 5 fish) and 30μM (146 segments; 6 fish) were affected when compared to stage-matched controls (152 segments; 6 fish). Filled arrows indicate pathfinding errors in dorsal projecting axons. Open arrows indicate pathfinding errors in ventral projecting axons. Arrowheads indicate errors in ventromedial projecting axons. Quantification shown in Fi and Fii is from a single representative experiment for each nicotine exposure paradigm (also see, Supplemental Fig.1). Asterisks in Fii denote statistical significance, p value < 0.05. Nicotine groups were compared against the control using a *post hoc* Dunn's test. Scale bars, 20 μm.

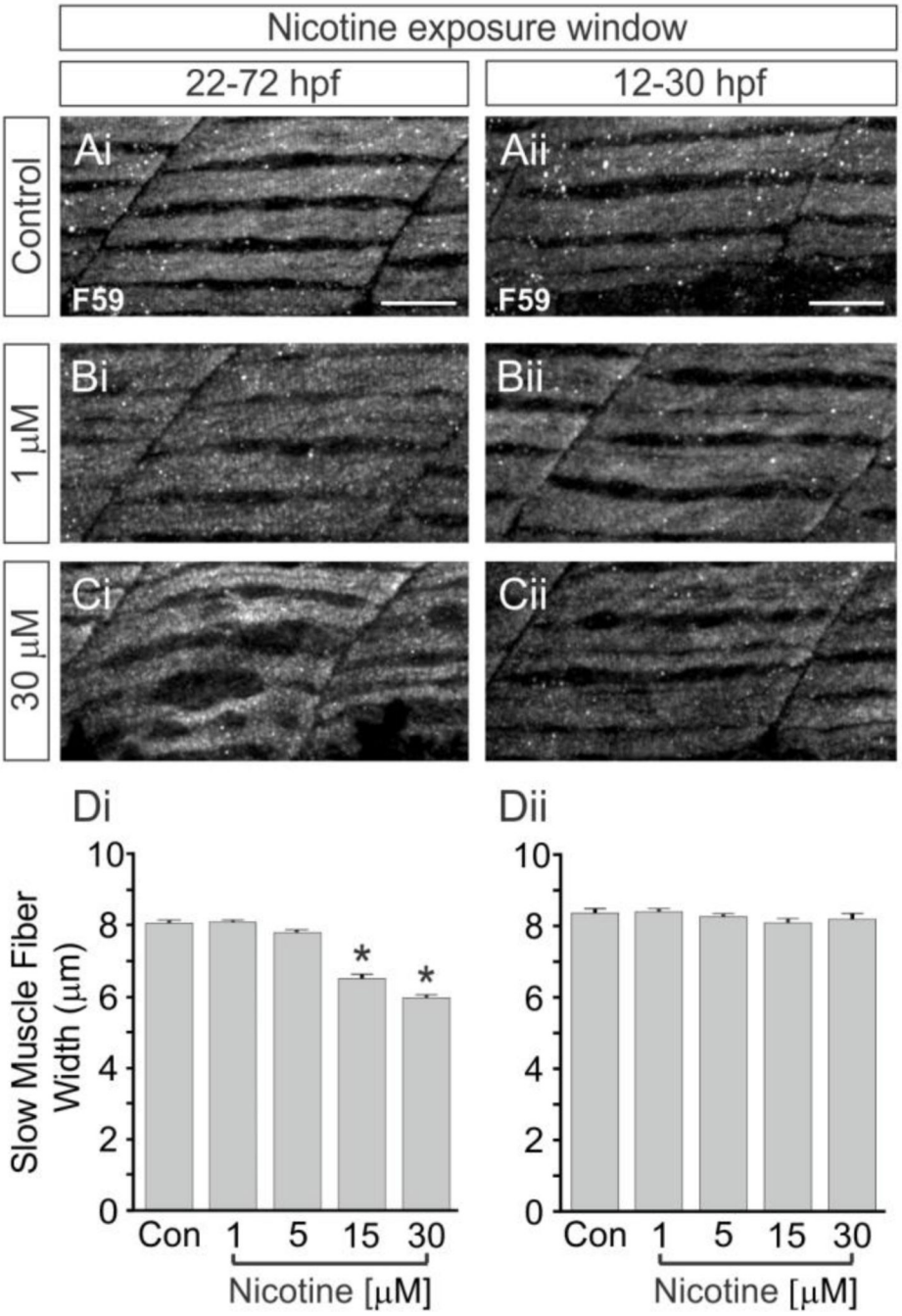

Figure 3. Morphology of slow muscle fibers following nicotine exposure

F59 immunoreactivity was used to reveal slow muscle fibers in 72-hpf zebrafish larvae exposed to varying concentrations of nicotine. Representative photomicrographs reveal multiple slow muscle fibers in the field of view from control larvae (Ai) and corresponding zebrafish larvae exposed to 1μM (Bi) 30μM (Ci) nicotine from 22–72 hpf. Di) Quantification of slow muscle fiber widths in 72 hpf zebrafish for exposure window between 22–72 hpf (control: 268 muscle fibers, 7 fish; 1μM: 237 muscle fibers, 7 fish; 5μM: 165 muscle fibers, 5 fish; 15μM: 207 muscle fibers, 7 fish; 30μM: 198 muscle fibers, 7 fish).

Aii–Cii) Same as in Ai–Ci but for nicotine exposure window between 12–30 hpf. Dii) Quantification of slow muscle fiber widths in 72-hpf zebrafish for exposure window between 12–30 hpf (control: 363 muscle fibers, 12 fish; 1μM: 256 muscle fibers, 10 fish; 5μM: 463 muscle fibers, 16 fish; 15μM: 398 muscle fibers, 13 fish; 30μM: 204 muscle fibers, 9 fish). Asterisk denotes statistical significance, p value < 0.05. Nicotine groups were compared against the control using a *post hoc* Holm-Sidak test. Scale bars, 20 μm.

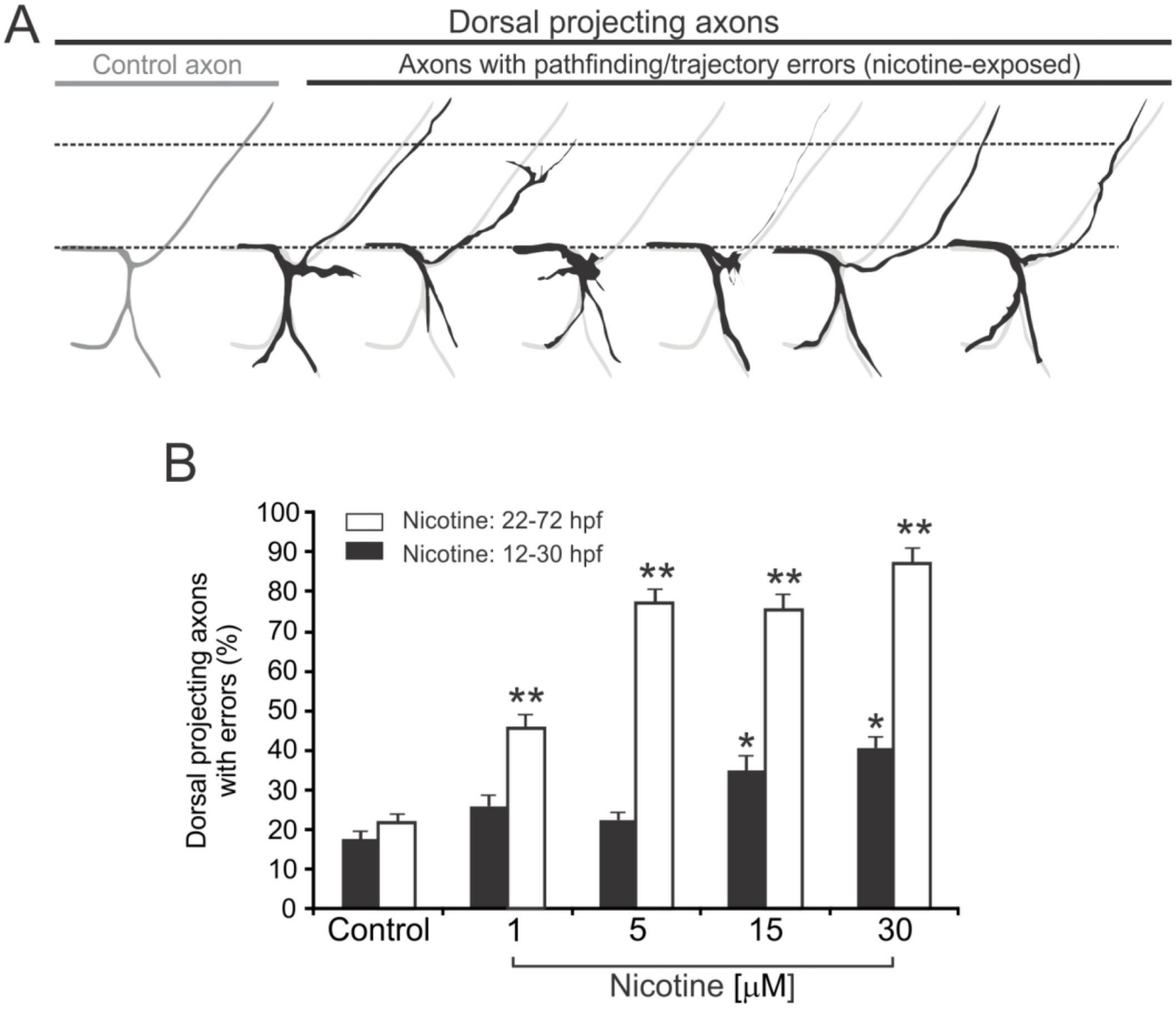

Figure 4. Effect of embryonic nicotine exposure on dorsal projecting SMN axons

A) Drawings depict a normal SMN axon projecting dorsally (grey) superimposed with observed nicotine-induced abnormal phenotypes (black). B) Dorsal projecting axons in 72-hpf zebrafish with abnormal phenotypes following a nicotine exposure between 12–30 hpf and 22–72 hpf. Dotted line denotes the boundaries of the spinal cord. The number of fish and hemisegments analyzed for each nicotine exposure paradigm is the same as in Table 1. Asterisk denotes statistical significance, p value < 0.05; double asterisks, p value < 0.001. Nicotine groups were compared against the control using a *post hoc* Holm-Sidak test. Cartoon is not drawn to scale.

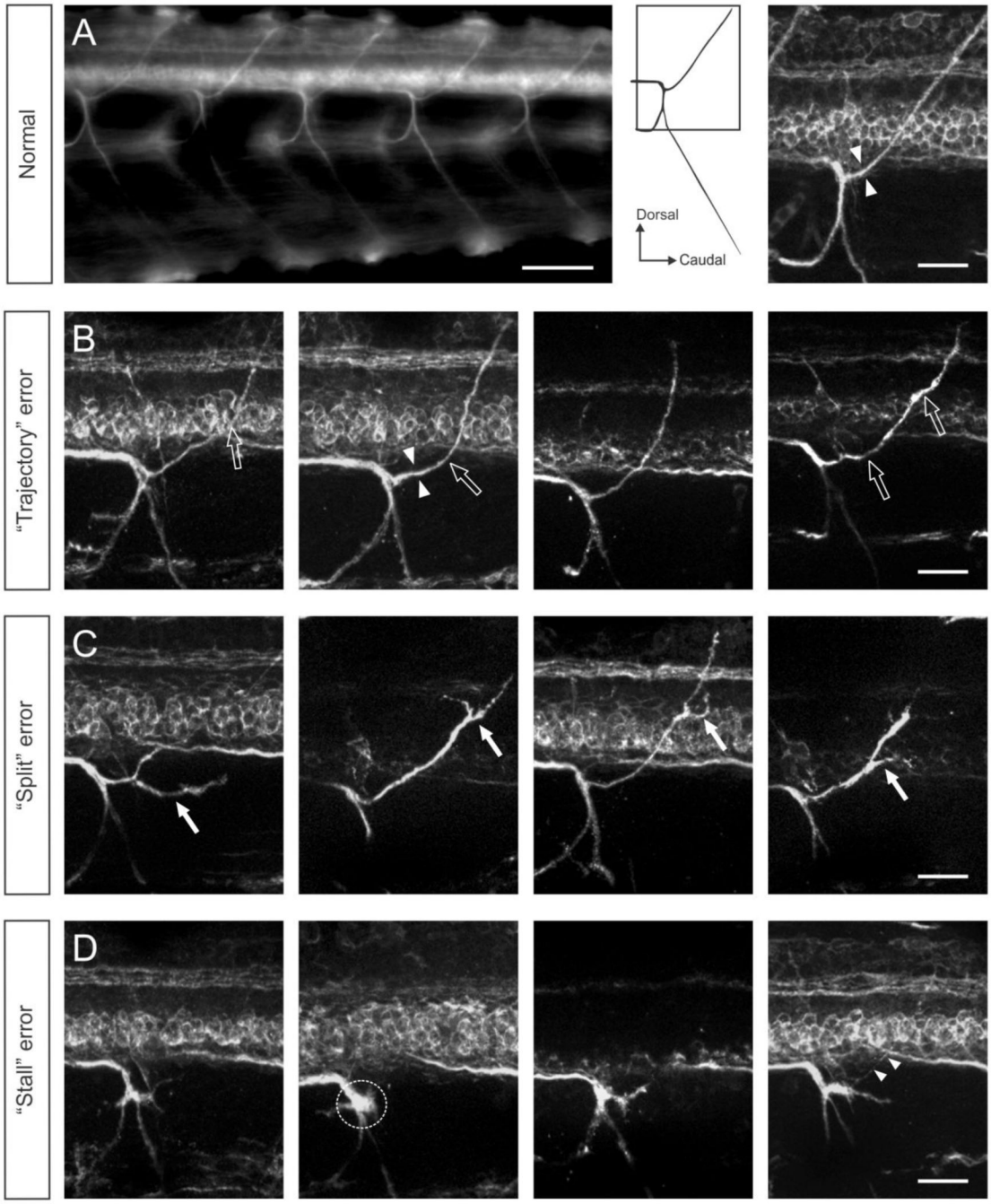

Figure 5. Three phenotypically distinct errors emerge on dorsal projecting SMN axons following embryonic nicotine exposure

A) Left, low magnification photomicrograph (zn5 immunoreactivity) reveals normal SMN axon trajectories (scale bar, 50 μm). Middle, diagram illustrates the normal trajectories of dorsal, ventral, and mediolateral motoneuron axons and the box outlines the region shown to the right. Right, high magnification photomicrograph reveals the normal trajectory path (arrowheads) of the dorsal projecting axon. Nicotine-induced phenotypes of dorsal projecting axons were categorized as "trajectory" (B), "split" (C) and "stall" (D) axonal errors. For each category, 4 representative example phenotypes are shown from different

nicotine exposed fish. B) “Trajectory” error refers to dorsal motoneuron axons that reach their dorsal most target but they drift (arrowheads) past their turning point and make sharp turns as they traject (open arrows). C) As the main nerve bundle of dorsal projecting SMN axons projects in the periphery, it splits (filled arrows) mainly into two different nerve fibers. D) Motor axons completely stall (dotted circle) as they exit the ventral root and fail to reach their dorsal most targets in the periphery. Arrowheads in D denote zn5-positive axons that have started to target dorsally after being stalled at the exit point. Scale bars, 20 μm.

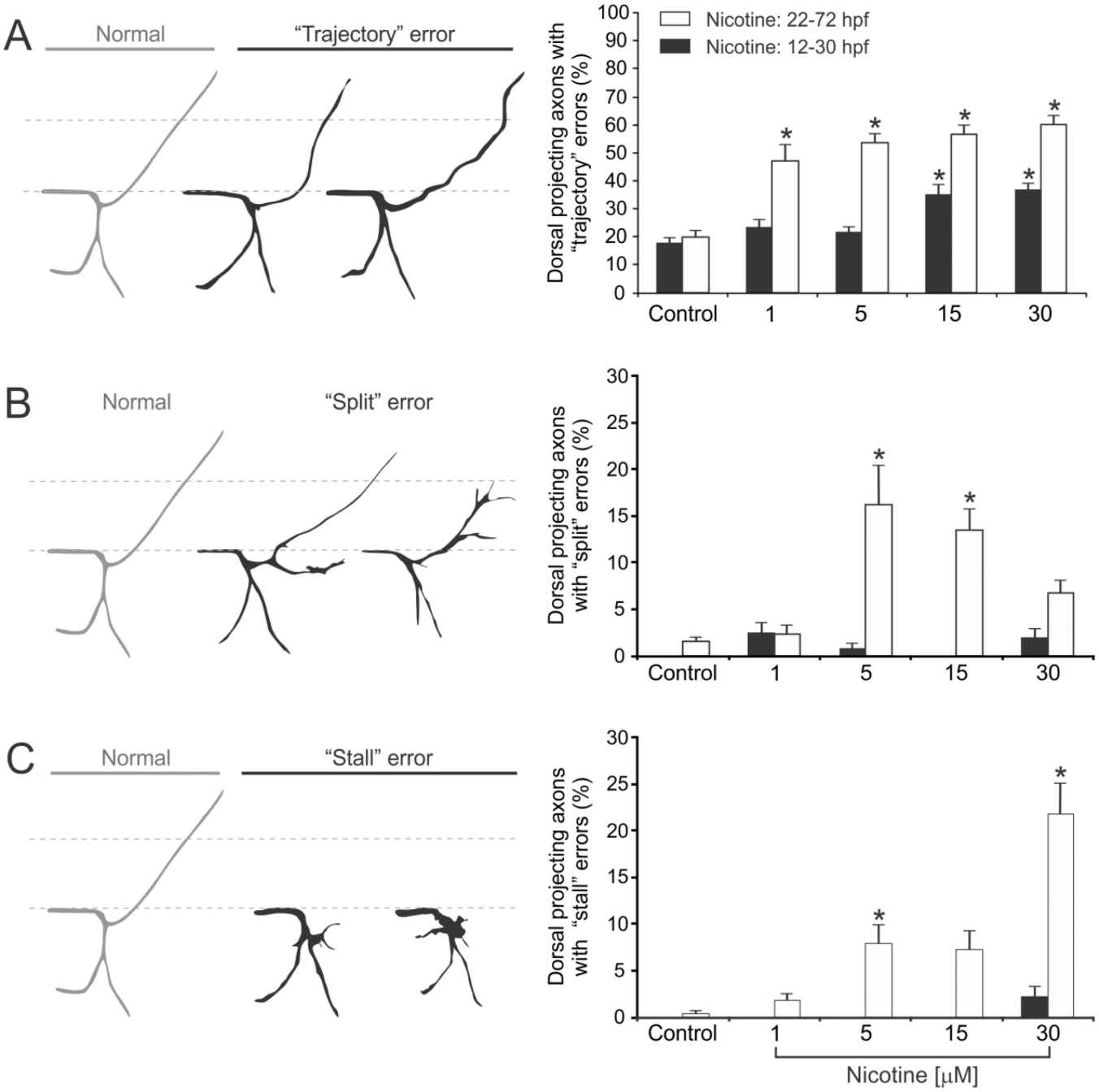

Figure 6. The nicotine-induced phenotypes of dorsal projecting SMN axons depend on the length of the exposure and nicotine concentration

A–C) Left, example cartoons depict one dorsal projecting SMN axons that has a normal projection and two abnormal phenotypes. Right, Quantification of the dorsal projecting SMN axons that have the corresponding abnormal phenotypes shown to the left ("trajectory" error, A; "split" axon error, B; "stall" axon error, C). Normal SMN axon phenotypes are shown in grey and abnormal phenotypes are shown in black. Dotted line denotes the boundaries of spinal cord. The number of fish and hemisegments analyzed for each nicotine exposure paradigm is the same as in Table 1. Dorsal is to the top and rostral is to the left.

Asterisk denotes statistical significance, p value < 0.05. Nicotine exposure groups were compared against the control using a *post hoc* Holm-Sidak (A) or Dunn's test (B and C). Cartoons are not drawn to scale.

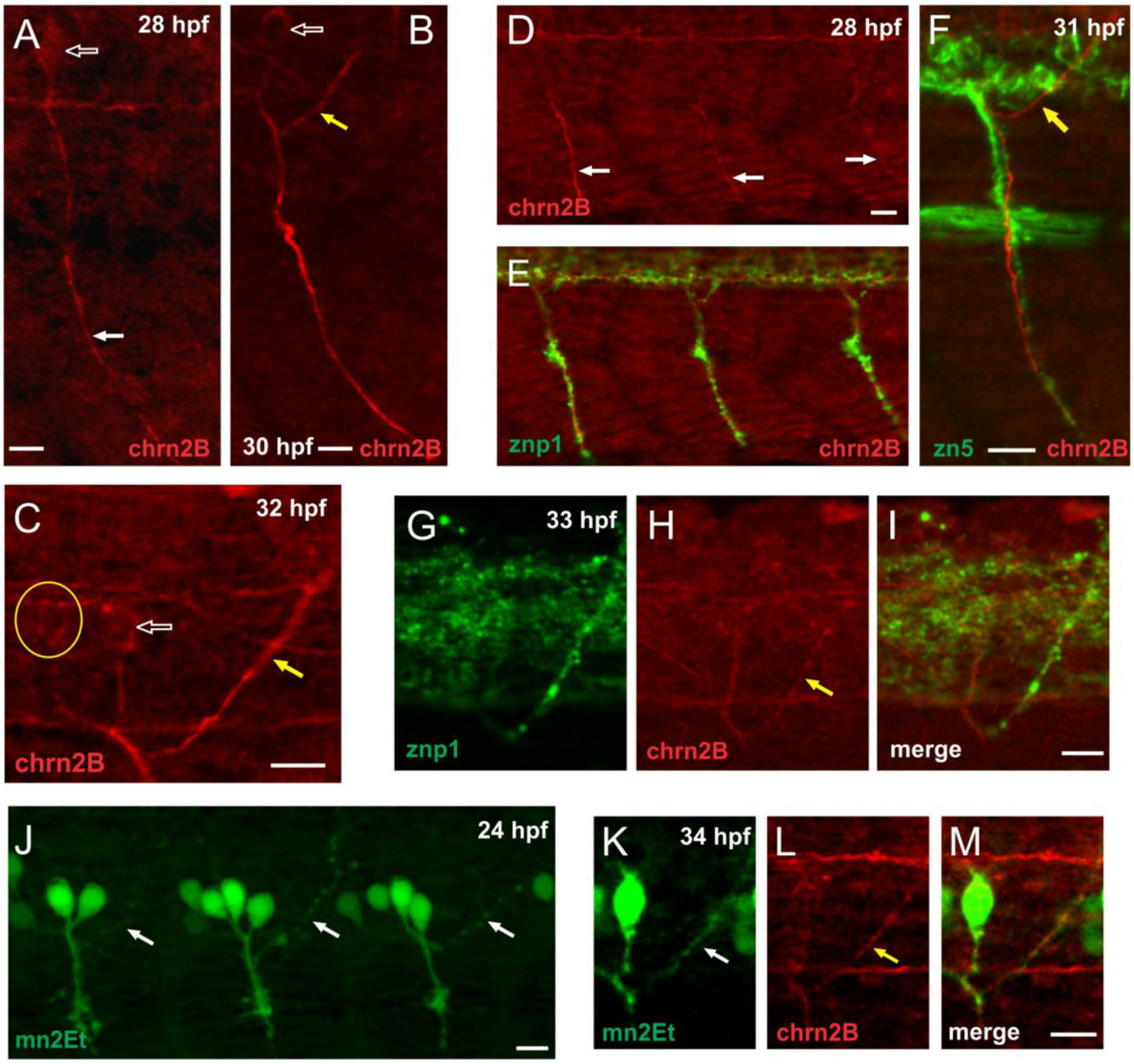

Figure 7. *anti-chrn2b* labels a subset of primary motoneuron somata and axons in zebrafish embryos

A) Left, image of CaP motoneuron detected by *anti-chrn2b* in a 28-hpf embryo. The white open and white arrows indicate the soma and axon of the putative CaP motoneuron, respectively (same in B). B) Image of CaP motoneuron axon and soma as well as a dorsal projecting axon (yellow arrow) detected by *anti-chrn2b* in a 30 hpf embryo. C) Image of 32-hpf embryo labeled with *anti-chrn2b*. Yellow arrow denotes the putative MiP motoneuron axon. White open arrow points to CaP motoneuron soma. Yellow circle highlights the presumptive soma of MiP motoneuron. D) Image from a 28-hpf embryo focusing on three ventral mytomes labeled with *anti-chrn2b*. E) Image from same fish in panel D now showing *anti-chrn2b* coupled with znp-1 labeling. F) Dual immunolabeling in a 31-hpf

embryo using *anti-chrn2b* and the zn5 antibody. The *anti-chrn2b* detected the ventral and dorsal projecting axons as shown from 1 body segment. The zn5 antibody labeled SMN somata and ventral projecting SMN axons. Note that the two antibodies detect two non-overlapping axons ventrally and dorsally only the earlier born MiP motoneuron axon (yellow arrow) projects into the periphery. G) Image of a dorsal projecting motoneuron axon labeled with znp-1 in a 33-hpf embryo. H) Image is from the same segment shown in panel G. The MiP axon was detected by *anti-chrn2b* (yellow arrow). I) Merging of panels G and H reveals colocalization of znp-1 and *anti-chrn2b* signal at the level of the dorsal projecting axon. J) Image of a 24-hpf, $parg^{mn2Et}$ embryo. White arrows denote putative MiP motoneuron axons. K) Image of a 34-hpf $parg^{mn2Et}$ embryo. White arrow denotes MiP axon. L) Image is from the same segment shown in panel K where the embryo was labeled with *anti-chrn2b*. Yellow arrow denotes dorsal projecting axon. M) Merging of panels K and L reveals co-localization of GFP signal and *anti-chrn2b* axonal signal at the level of the MiP motoneuron axon. See Supplemental Table 1 for number of fish analyzed for each developmental time point. Scale bars; 10 μm.

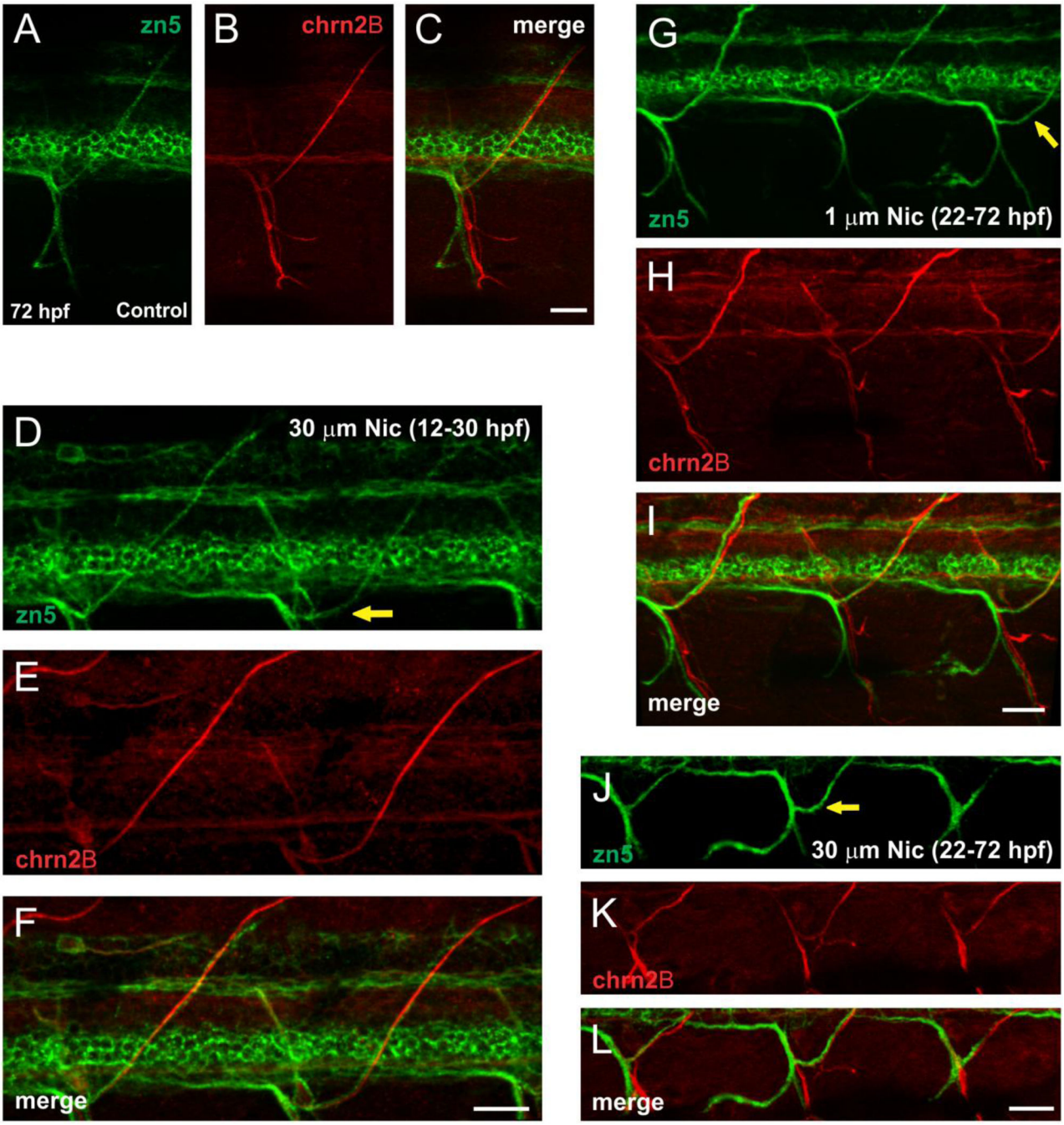

Figure 8. Simultaneous examination of nicotine-induced effects onto primary and secondary motoneuron axons

A–C) Representative photomicrographs from a 72-hpf control larva labeled with the zn5 antibody and *anti-chrn2b*. Photomicrographs from 3 different 72-hpf larvae labeled with the zn5 antibody and *anti-chrn2b* and exposed to either 30μM nicotine from 12–30 hpf (D–F), 1μM nicotine from 22–72 hpf (G–I) or 30μM nicotine from 22–72 hpf (J–L). Yellow arrows in each exposure example denote SMN axons that extended too far caudally before turning dorsally. See Supplemental Table 1 for number of fish analyzed for each nicotine exposure paradigm. Scale bars; 20 μm.

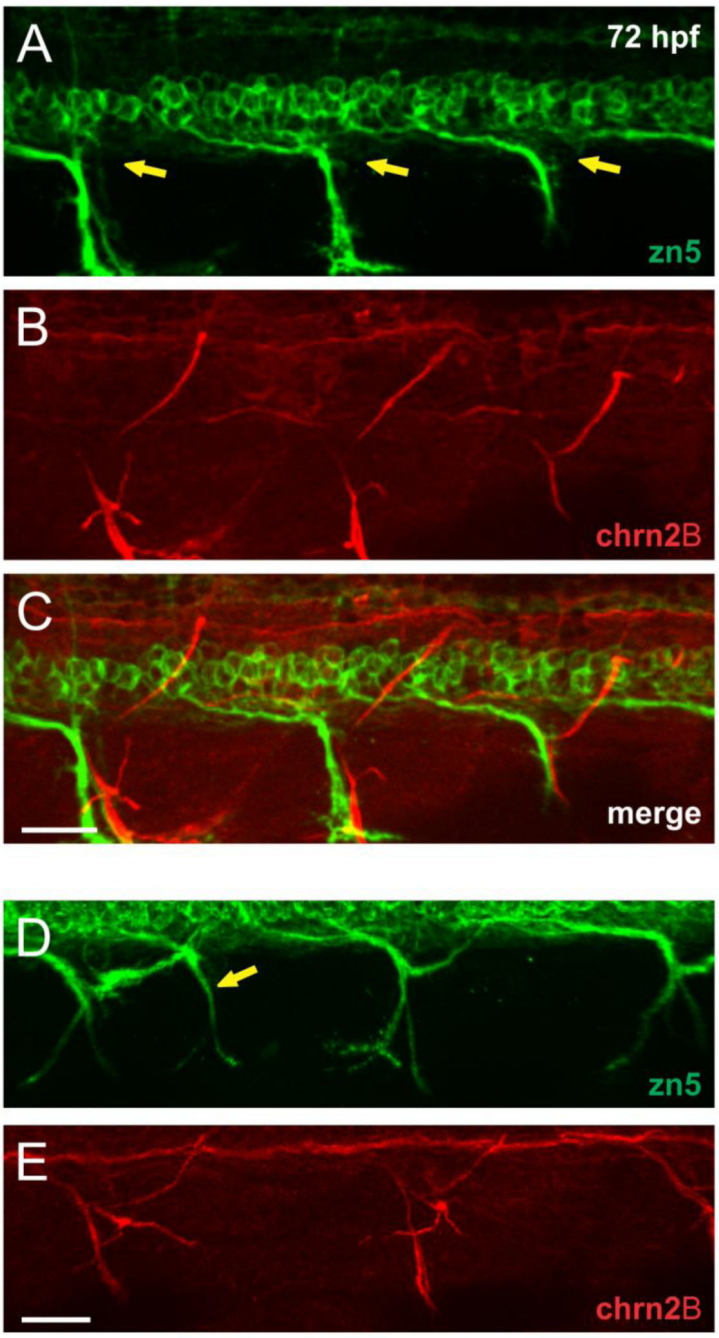

Figure 9. The nicotine-induced "stall" and "duplication" errors are specific to SMN axons

A–C) Photomicrographs of a 72-hpf larva exposed to 30μM nicotine from 22–72 hpf. The zn5-positive SMN dorsal projecting axons (yellow arrows in A) have not extended into the periphery and appear to have stalled. B–C) *Anti-chrn2b* antibody detects MiP motoneuron axons in the periphery whereas zn5-positive SMN axons have not extended into the periphery. D) Image of a 72-hpf larva exposed to 30μM nicotine from 22–72 hpf. There is a duplicated SMN nerve root shown by the yellow arrow. E) Photomicrograph of the fish shown in D labeled with *anti-chrn2b*. The anti-*chrn2b-positive* dorsal and ventral projecting

axons extended out into the periphery in these 3 consecutive segments. There was no ventral nerve root duplication that matched the zn5-positive one in panel D (yellow arrow). See Supplemental Table 1 for number of fish analyzed for each nicotine exposure paradigm. Scale bars; 20 μm.

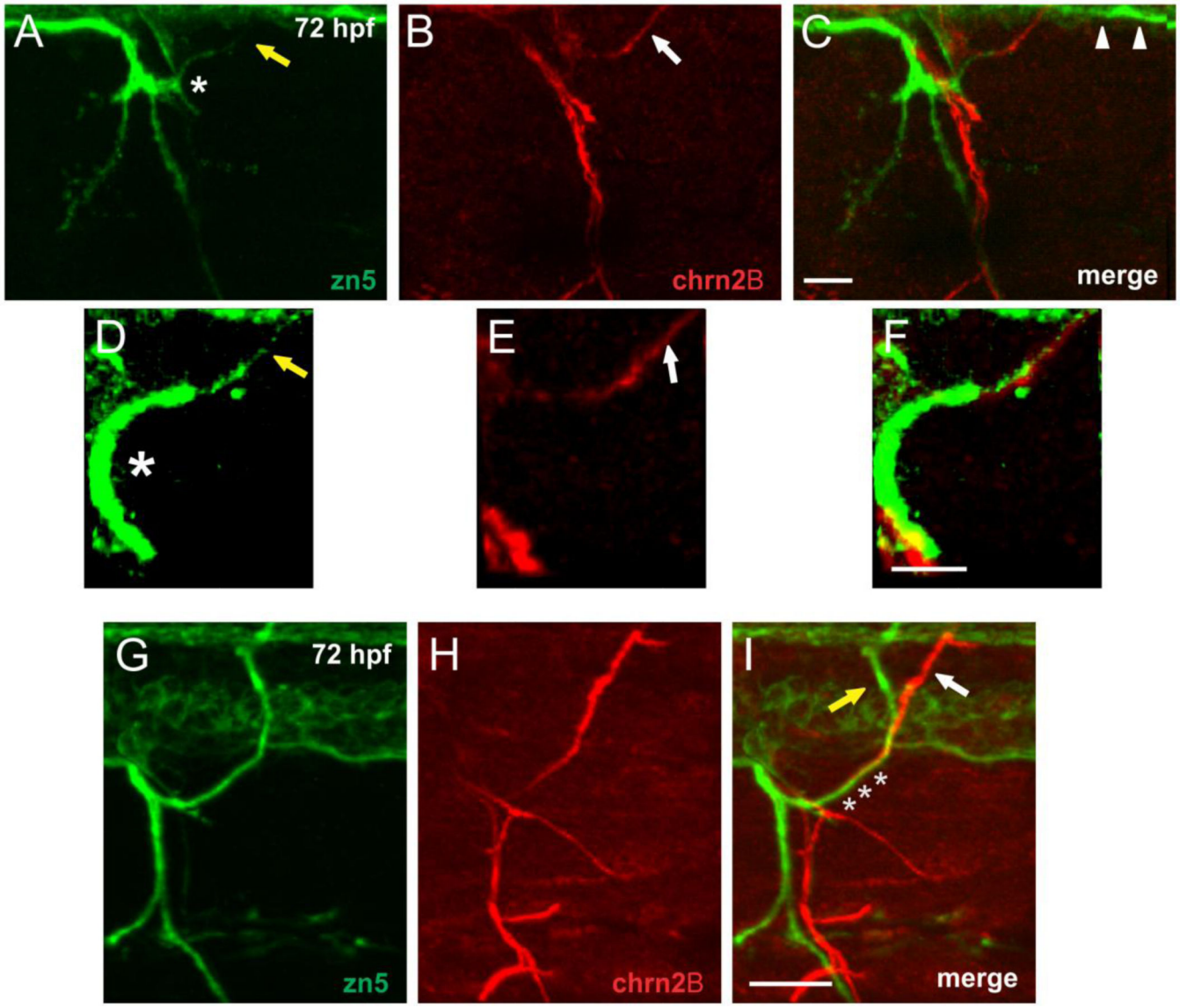

Figure 10. Differential effects along the motoneuron axon path following nicotine exposures

A–C) Photomicrographs of a 72-hpf larva labeled with zn5 and *anti-chrn2b* capture motoneuron axon extension within 1 segment just below spinal cord (ventral edge of spinal cord indicated by white arrowheads). This larva was exposed to 30μM from 22–72 hpf. Note that the zn5-positive axon appears stalled at this magnification whereas the *anti-chrn2b*-positive axon (white arrow in panel B) takes a dorsal trajectory. Yellow arrow in A points to a weak zn5 signal; likely a few axons which have migrated dorsally. The asterisk in A provides a reference point of the magnified area in D–F. D–F) The images in A–C shown at higher magnification. Zn5-positive axons appear to migrate to the periphery using the *anti-chrn2b* - positive axon as a guide. Conventions are the same as in A–C. G–I) Photomicrographs of a 72-hpf larva labeled with zn5 and *anti-chrn2b*. This larva was exposed to 30μM from 22–72 hpf. Zn5-positive axons appear to use the *anti-chrn2b*-positive axon as a guide when navigating below spinal cord (marked by asterisks). Once in the distal dorsal periphery, the zn5-positive axons exhibit pathfinding errors (yellow arrow) whereas

the *anti-chrn2b*-positive axon targeted the periphery using a slightly different dorsal path (white arrow). The zebrafish larva presented under panels A–F was presented earlier in Fig. 2Ei. See Supplemental Table 1 for number of fish analyzed for each nicotine exposure paradigm. Scale bars; 10 μm in C and F, 20 μm in I.

Table 1

Examination of different secondary motoneuron axon trajectories at 72-hpf following nicotine exposure during embryogenesis.

Exposure		Normal axons (%)			Analyzed Hemisegments[a]
		Dorsal	Ventral	Mediolateral	
12–30 hpf[b]					
Control		82.2 ± 2.3	97.5 ± 0.9	97.2 ± 1.2	145 (6)
Nicotine	1μM	74.0 ± 2.9	96.2 ± 1.4	96.6 ± 1.4	163 (7)
	5μM	77.7 ± 2.2	96.4 ± 2.8	99.0 ± 0.8	155 (6)
	15μM	64.9 ± 3.7*	96.2 ± 1.2	96.9 ± 1.0	121 (5)
	30μM	59.3 ± 2.8*	93.1 ± 1.4	89.2 ± 3.0	147 (6)
22–72 hpf[c]					
Control		78.8 ± 3.3	93.5 ± 2.3	96.2 ± 2.0	260 (10)
Nicotine	1μM	53.4 ± 3.3**	86.8 ± 2.3	95.2 ± 1.6	316 (11)
	5μM	22.7 ± 3.4**	83.9 ± 2.3	88.6 ± 2.6	223 (8)
	15μM	22.9 ± 4.2**	80.0 ± 4.2*	68.4 ± 4.8*	268 (10)
	30μM	12.9 ± 3.8**	80.1 ± 5.5*	68.0 ± 7.6*	232 (9)

[a] The number of embryos analyzed is shown in the parenthesis.

[b] Statistical analysis was performed using Kruskal-Wallis one-way ANOVA on ranks.
Dorsal: $H_{(4)}=16.859$ $(p=0.002)$; Ventral: $H_{(4)}=5.208$ $(p=0.267)$; Mediolateral: $H_{(4)}=7.119(p=0.130)$.

[c] Statistical analysis was performed using one-way ANOVA or Kruskal-Wallis one-way ANOVA on ranks. Dorsal: $F_{(4,43)}=60.494(p<0.001)$; Ventral: $F_{(4,43)}=3.496(p=0.015)$; Mediolateral: $H_{(4)}=23.671(p<0.001)$.

Statistical significance is denoted by *p <0.05 and **p<0.001 following *post hoc* multiple comparisons tests of nicotine treatments against the control group (See details in Materials and Methods).